First posted online on 6 March 2018 as 10.1242/dev.161208
Access the most recent version at http://dev.biologists.org/lookup/doi/10.1242/dev.161208

Genome-wide strategies identify downstream target genes of connective tissue-associated transcription factors

Mickael Orgeur[1,2,3], Marvin Martens[3], Georgeta Leonte[2,4], Sonya Nassari[3], Marie-Ange Bonnin[3], Stefan T. Börno[2], Bernd Timmermann[2], Jochen Hecht[2,5,6,7], Delphine Duprez[3,*,#] and Sigmar Stricker[1,2,*,#].

[1] Freie Universität Berlin, Institute of Chemistry and Biochemistry, Thielallee 63, 14195 Berlin, Germany

[2] Max Planck Institute for Molecular Genetics, Ihnestr. 63-73, 14195 Berlin, Germany

[3] Sorbonne Universités, UPMC Univ. Paris 06, CNRS UMR 7622, Inserm U1156, IBPS-Developmental Biology Laboratory, 9 Quai Saint-Bernard, 75005 Paris, France

[4] Freie Universität Berlin, Institute of Biology, Königin-Luise-Str. 1-3, 14195 Berlin, Germany

[5] Berlin-Brandenburg Center for Regenerative Therapies (BCRT), Charité Universitatsmedizin, Augustenburger Platz 1, 13353 Berlin, Germany

[6] Centre for Genomic Regulation (CRG), The Barcelona Institute for Science and Technology, Dr. Aiguader 88, 08003 Barcelona, Spain

[7] Universitat Pompeu Fabra (UPF), 08002 Barcelona, Spain

[*] Equal contribution

[#] Corresponding authors

Sigmar Stricker: sigmar.stricker@fu-berlin.de; +49 30 8387 5799

Delphine Duprez: delphine.duprez@sorbonne-universite.fr; +33 1 4427 2753

Keywords: chicken model, limb development, connective tissue differentiation, extracellular matrix, signalling pathways, transcription factors, transcriptional regulatory network.

Summary Statement

Global profiling of five transcription factors associated with connective tissue subtypes reveals molecular signatures regulated during limb development and provides a data resource for future studies of connective tissue formation.

List of abbreviations

3F, triple-FLAG; chMM, chick micromass; CDS, coding sequence; ChIP-seq, chromatin immunoprecipitation sequencing; CT, connective tissue; DE, differentially expressed; ECM, extracellular matrix; FDR, false-discovery rate; GO, gene ontology; IDR, irreproducibility discovery rate; padj, Benjamini-Hochberg adjusted p-value; PCA, principal components analysis; rlog; regularized logarithm; RNA-seq, whole transcriptome sequencing; TF, transcription factor; TFBS, transcription factor binding sites; TPM, transcripts per million; TSS, transcriptional start site.

Abstract

Connective tissues support organs and play crucial roles in development, homeostasis and fibrosis, yet our understanding of their formation is still limited. To gain insight into the molecular mechanisms of connective tissue specification, we selected five zinc finger transcription factors - OSR1, OSR2, EGR1, KLF2 and KLF4 - based on their expression patterns and/or known involvement in connective tissue subtype differentiation. RNA-seq and ChIP-seq profiling revealed a set of common genes regulated by all five transcription factors, which we propose as connective tissue core expression set. This common core was enriched in genes associated with axon guidance and myofibroblast signature, including fibrosis-related genes. In addition, each transcription factor regulated a specific set of signalling molecules and extracellular matrix components. This suggests a concept whereby local molecular niches can be created via the expression of specific transcription factors impinging on the specification of local microenvironments. The regulatory network established here identifies common and distinct molecular signatures of limb connective tissue subtypes, provides novel insight into the signalling pathways governing connective tissue specification, and serves as a resource for connective tissue development.

Introduction

Connective tissue (CT) is one of the main components of the body essential for supporting tissues and organs, in part via the production of tissue-specific extracellular matrix (ECM). The term of CT gathers together an ensemble of tissues such as specialized CT (cartilage and bone), soft CT (adipose tissue and vasculature) and dense CT. Dense CT can be divided into regular CT (tendon and ligament) and irregular CT (loose CT surrounding or within organs such as muscle CT) (Nassari et al., 2017a). Regular and irregular CTs are an integral part of the musculoskeletal system. Muscle CT is pivotal for the mechanical properties of muscle and is structurally continuous with the tendons, which finally transmit force to the skeleton. Dysregulation of CT homeostasis leads to fibrosis, which is observed during pathological tissue repair or healing processes and in cancer (Kalluri, 2016). Although fibrosis is a common research subject, normal CT formation during development remains to date poorly investigated.

The appendage of vertebrate embryos is an excellent model system for analysing tissue differentiation and cellular interactions during development. In limbs, cells forming the skeleton, as well as regular and irregular CTs, are derived from the lateral plate mesoderm, while myogenic cells originate from the somites (Chevallier et al., 1977; Christ et al., 1977). Classical embryological experiments have shown that limb patterning is dependent on lateral plate-derived CTs that provide instructive cues to guarantee correct muscle, nerve and vessel formation (Gaut and Duprez, 2016; Kardon, 1998; Lance-Jones and Dias, 1991; Michaud et al., 1997). The nature of these cues is so far mostly elusive, but it is assumed that a key role is played by specific ECM in combination with locally produced paracrine signaling factors (Hasson, 2011; Nassari et al., 2017a). Altogether, CT cells appear as key players creating local microenvironments that contain permissive and/or instructive cues for organ patterning.

Specification, differentiation and function taken by a progenitor cell encompasses dramatic transcriptional and finally phenotypic changes that differ for each cell/tissue type. Lineage-

specific genetic programs consist in a fine-tuning between the repression and the expression of a given set of genes in response to extrinsic and intrinsic signals at a specific location and/or at a precise time (Heinz et al., 2015). Progenitor cells are specified and induced to differentiate along a certain lineage upon activation of lineage-specific key transcription factors (TFs) that drive specific transcriptional programs (Spitz and Furlong, 2012). As a consequence, the differentiating progenitor cells express lineage-specific genes that reinforce lineage commitment, as well as providing unique characteristics to the specific cell type and the tissue it gives rise to. While master TFs governing cell-type specific gene expression programs have been identified for cartilage (SOX9), bone (RUNX2) and muscle (MYF5, MYF6, MYOD) development (Braun and Gautel, 2011; Kronenberg, 2003), knowledge is sparse for dense CT. CT is mostly identified by gene/protein expression associated with CT function. Irregular CT is associated with type-III and -VI collagens, while regular CT (tendon/ligament) is characterized by the expression of structural and functional components such as type-I and -XII collagens or Tenomodulin (TNMD) (Gaut and Duprez, 2016; Huang et al., 2015). Few TFs specific to CT lineages have been identified. Scleraxis (SCX) is to date the best marker for tendon cells, however it is not necessary for development of most tendons (Murchison et al., 2007; Schweitzer et al., 2001). Early growth response 1 (EGR1) is involved in type-I collagen production in chick and mouse developing tendons (Lejard et al., 2011). Moreover, EGR1-forced expression is sufficient to induce the expression of tendon-associated genes in murine mesenchymal stem cells (Guerquin et al., 2013). TBX4 and TBX5 are expressed in limb irregular CT, TCF4 (TCF7L2) is expressed in irregular CT associated with muscle, but they have no obvious role in CT differentiation (Hasson et al., 2010; Kardon et al., 2003). In contrast, Odd-skipped related 1 and 2 (OSR1 and OSR2) are expressed and involved in irregular CT differentiation during chick and mouse limb development (Nassari et al., 2017b; Stricker et al., 2006; Stricker et al., 2012; Vallecillo-García et al., 2017). Moreover, TBX4, TBX5, TCF4 and

OSR1 are involved in the non-cell autonomous regulation of muscle patterning by CT (Hasson et al., 2010; Mathew et al., 2011; Vallecillo-García et al., 2017).

Here, we present a comprehensive analysis of five selected zinger finger TFs addressing the molecular mechanisms underlying CT differentiation and function during chick limb development. OSR1, OSR2 and EGR1 were chosen based on their demonstrated contribution in irregular and regular CT development, respectively. KLF2 and KLF4 (Krüppel-like factor 2 and 4) were chosen based on their expression patterns in CT associated with tendons, although their role in limb development is presently not elucidated. We combined whole transcriptome sequencing (RNA-seq) and chromatin immunoprecipitation sequencing (ChIP-seq) to identify the gene regulatory programs downstream of the five selected CT-associated TFs. This allowed us to design a novel and unique regulatory network underlying CT differentiation and to identify common and specific target genes that are regulated during this process. This study furthermore provides a resource framework for future analyses of CT development.

Results

Limb expression patterns of CT-associated TFs

We first re-examined the gene expression patterns of the five selected CT-associated TFs in chick limbs during development. Consistent with previous observations (Stricker et al., 2006; Stricker et al., 2012), *OSR1* and *OSR2* were expressed in dorsal and ventral limb regions of E4.5 chick embryos (Fig. 1A,B), overlapping in part with the expression domains of *SCX* and *MYOD*, which labelled tendon and myogenic cells, respectively (Fig. 1C,D). Although displaying overlapping domains, *OSR1* and *OSR2* were previously shown to be exclusive to *PAX3*$^{+}$ and *MYOD*$^{+}$ cells and to be partially co-expressed with *SCX*$^{+}$ cells in limbs of E4 chick embryos (Stricker et al., 2012). At E9.5, when the final pattern of the musculoskeletal system is set, both *OSR1* and *OSR2* were not expressed in *SCX*$^{+}$ tendons (Fig. 1E-J), but rather expressed in muscle CT, interstitial to muscle fibres (Fig. 1F-I). Of note, *OSR1* and *OSR2* appeared to be expressed in all limb muscles, yet with differential levels (Fig. 1F,G) (Nassari et al., 2017b). *OSR1* was also detected in CT surrounding individual muscles and in the dermis (Fig. 1F), as it was reported for the mouse (Vallecillo-García et al., 2017). We concluded that while *OSR1* and *OSR2* were expressed in a subset of tendon progenitors (Stricker et al., 2012), their expression was excluded from mature tendons and became specific to irregular CT. In contrast to both *OSR* transcripts, *EGR1*, *KLF2* and *KLF4* were not detected in E4.5 limb buds, but were first observed in E5.5 limbs (Antin et al., 2010; Lejard et al., 2011). *EGR1* was expressed in tendons, close to muscle attachments (Fig. 1E,E',K-M), as previously described (Lejard et al., 2011), while *KLF2* and *KLF4* transcripts delineated *SCX*$^{+}$ tendons of the knee of E9.5 chick embryos (Fig. 1N-S). In summary, *OSR1* and *OSR2* label irregular CT, whereas *EGR1*, *KLF2* and *KLF4* are expressed in different regions of regular CT in developing chick limbs.

CT-associated TFs influence differentiation of limb mesenchymal progenitors

To analyse the functionality of the five TFs towards CT differentiation, we chose the chick micromass (chMM) explant model (Fig. 2A). In this three-dimensional culture model, limb bud cells behave close to the *in vivo* situation and differentiate into the mesenchymal lineages observed in native limb buds (Ahrens et al., 1979). We tested the ability of the five TFs to shift cell differentiation in chMM cultures via their overexpression with RCAS replication-competent retroviruses. This retroviral system allows for high transfection efficiency with mild overexpression of genes of interest, which has been shown to be in a physiological range when compared to endogenous expression in native limb buds, and has been tested for cell differentiation, transcriptome and chromatin binding analyses before (Ibrahim et al., 2013). Due to the absence of specific antibodies targeting each of the selected chicken TFs, we used the triple-FLAG (3F) tag that was fused C-terminally to the coding sequence (CDS) of each TF. Overexpression of the recombinant TFs was monitored by immunohistochemistry and Western blot analysis against the 3F tag (Fig. S1). While the overall morphology of the chMM cultures remained unchanged across all conditions, cartilage differentiation was affected upon TF overexpression (Fig. 2B,C). In agreement with previous observations (Stricker et al., 2012), OSR1 and OSR2 overexpression reduced chondrogenic matrix production by 58% and 67%, respectively, compared to control cultures (Fig. 2C,D). Similarly, KLF2 and KLF4 overexpression induced a reduction of cartilage nodule formation, but to a lower extent compared to OSR1 and OSR2 (Fig. 2C,D). EGR1 was the only factor that increased chondrogenic matrix production within the chMM cultures (Fig. 2C,D). Quantitative RT-PCR analysis of transcript levels of cartilage-associated genes, *SOX9* and *COL2A1*, confirmed the inhibitory effect of OSR1, OSR2, KLF2 and KLF4 overexpression, as well as the positive effect of EGR1 overexpression on cartilage differentiation (Fig. 2E-G). EGR1 overexpression increased the expression of the tendon differentiation marker, *TNMD*, while not affecting that of the irregular CT markers *COL3A1* and *COL6A1* (Fig. 2E). Overexpression of KLF2, but not

that of KLF4, increased the expression levels of the tendon markers *SCX* and *TNMD* (Fig. 2F). Both KLF factors also increased *COL6A1* expression (Fig. 2F). OSR2 overexpression increased the expression of the CT markers *COL3A1* and *COL6A1*, while OSR1 overexpression only affected *COL3A1* expression (Fig. 2G). In summary, the TFs had different outcome on CT differentiation. OSR1 and OSR2 drove undifferentiated limb mesenchymal cells towards irregular CT differentiation at the expense of cartilage differentiation. EGR1 induced tendon and cartilage marker expression, while not affecting irregular CT marker expression. KLF2, but not KLF4, promoted the expression of tendon markers, while both KLF factors increased *COL6A1* expression and decreased *COL2A1* expression. In conclusion, all five TFs proved functional in this model towards an effect on CT cell differentiation.

Transcriptome analysis reveals similar regulatory functions between CT-associated TFs

To gain insight into regulatory functions of the five TFs, transcriptome analysis was performed by RNA-seq of two independent biological replicates of 5-day chMM cultures overexpressing each of the TFs. Principal components analysis (PCA) and hierarchical clustering of the Euclidean distances on global gene expression profiles depicted a separation between the TF-overexpressing chMM cultures (Fig. 3A, Fig. S2). Consistent with their similar expression domains in irregular CT, the gene expression profiles induced upon OSR1 and OSR2 overexpression were grouped together. In contrast, the gene expression profiles retrieved upon overexpression of the tendon-related TFs, EGR1, KLF2 and KLF4, were gathered together in a second group. Consistent with their distinct expression domains associated with tendons, KLF2 and KLF4 profiles were more similar to each other than to EGR1. In summary, the gene expression profiles retrieved in the chMM cultures are in line with the limb expression patterns of the five TFs in the different CT subtypes.

We identified between 1,369 and 2,907 differentially expressed (DE) genes for each TF-overexpressing culture compared to control cultures (Fig. S3), resulting in a total of 10,712 DE genes for all TFs that corresponded to 4,298 non-redundant genes (Fig. 3B, Table S1). While 1,487 (34.6%) DE genes were specific to a single TF, 2,811 (65.4%) DE genes were shared by at least two TFs (Fig. 3B). In addition, 726 (16.9%) DE genes were identified in all TF-overexpressing culture conditions (Fig. 3B). This indicates that the five TFs significantly share a core of common regulatory targets, despite being expressed in distinct CT subtypes (SuperExactTest, $P < 10^{-10}$). When performing a fold-change comparison (i.e. whether the gene is upregulated or downregulated), only 48 (1.7%) DE genes that were shared by at least two TFs were identified as being regulated in opposite directions between the subset of TFs misregulating them (Fig. S4). Therefore, the TFs did not have only similarities in the genes they regulated, but also in the manner these genes were affected.

Based on their expression patterns across all culture conditions, the 4,298 non-redundant DE genes were clustered by using *K*-means and partitioned into 8 groups (Fig. 3C). Gene ontology (GO) analysis was then performed to identify potential biological processes enriched within each cluster (Fig. 3D). Genes downregulated by all five TFs were mainly involved in protein localization, ion transport and metabolic processes (Fig. 3C,D: cluster I). Genes upregulated by all five TFs were related to metabolic processes, gene expression, cellular component organization and several GO terms associated with the regulation of cell signalling and communication (Fig. 3C,D: cluster VIII). The clusters II, III, IV and V corresponded to genes upregulated specifically by one TF or by two closely related paralogous TFs (OSR1/OSR2 or KLF2/KLF4) (Fig. 3C). Genes in these clusters were mainly enriched for cell differentiation, mesoderm development, cell signalling/communication and biological/cell adhesion (Fig. 3D). Genes downregulated upon OSR1 and OSR2 overexpression were enriched for biological processes related to chondrogenesis (Fig. 3C,D: cluster VI), which was consistent with their anti-chondrogenic effect in chick cell cultures (Fig. 2C,D,G) (Stricker et al., 2012). In summary,

the five CT-associated TFs differentially regulate the expression of genes mainly related to cell differentiation, signalling and adhesion. Thereby, they show a significant degree of overlapping regulatory function despite belonging to distinct CT subtypes.

Molecular signatures downstream of the five TFs

Given that a high proportion of genes upregulated by the selected CT-associated TFs was involved in signal transduction and biological adhesion, we performed a signalling pathway enrichment analysis on the complete set of DE genes identified for each TF. Of particular interest, signalling pathways related to ECM components, such as integrin and cadherin signalling pathways, Wnt signalling, CCKR signalling and angiogenesis were enriched across all five TFs (Fig. 4A). Additional pathways were specifically enriched by a subset of TFs. TGF-β signalling pathway was identified upon overexpression of OSR1, OSR2 and KLF2, while Notch signalling pathway was enriched for both KLF2 and KLF4 DE genes (Fig. 4A). "Axon guidance mediated by netrin" and "cytoskeletal regulation by Rho GTPase" pathways were enriched in both OSR1- and OSR2-associated DE genes (Fig. 4A). When comparing the averaged fold-change across all TFs for each DE gene, it appeared that DE genes within each aforementioned pathway were significantly upregulated (Fig. 4B: median log2 fold change close to 1; Wilcoxon rank-sum test, $P < 0.05$). This tendency was not observed for the remaining non-DE genes associated with these signalling pathways (Fig. 4C: median log2 fold change close to 0). Nevertheless, a proportion of DE genes appeared rather downregulated for the integrin and TGF-β signalling pathways (Fig. 4B: lower whisker). This corresponded to a set of genes mainly repressed by both OSR factors (Fig. S5). Most of these genes encode collagens and BMP/GDF signalling molecules associated with cartilage and bone development, which is consistent with the anti-chondrogenic function of OSR1 and OSR2 (Fig. 2C,D,G) (Stricker et al., 2012). In agreement with the signalling pathway enrichment analysis, overrepresentation

test on the 4,298 non-redundant DE genes highlighted ECM, membrane and cytoskeleton cellular components (Fig. 4D). Altogether, gene expression profiling of chMM cultures overexpressing each TF supports a core of common regulatory functions across all TFs related to cell signalling, communication and ECM-based cell adhesion. In addition, each TF (or paralogous TFs) also appear to be involved in e.g. regulation of individual signalling pathways, which could contribute to create a local microenvironment related to each CT subtype.

Establishing a regulatory chromatin map of the chMM system

We then explored the chromatin landscape of the chMM system by building a comprehensive map of promoter and enhancer regulatory domains. ChIP-seq was performed in two independent biological replicates of 5-day chMM cultures overexpressing no recombinant protein, corresponding to the control conditions used for RNA-seq, to reveal the unbiased chromatin landscape independently of TF overexpression. Mono-, bi- and tri-methylation of H3K4 (H3K4me1/2/3) were assessed to identify promoter and enhancer domains, while H3K27ac and H3K27me3 were used to distinguish between regions of transcriptional activity and facultative heterochromatin, respectively (Fig. S6A) (Kim and Shiekhattar, 2015). This identified 20,427 promoters and 55,597 enhancers (Fig. S6B,C). Surprisingly, we observed a globally decreased enrichment of active chromatin marks H3K4me3 and H3K27ac compensated by an increased signal of the repressive mark H3K27me3 at the transcriptional start site (TSS) positions of DE genes, as compared to their genome-wide levels or a set of randomly selected genes of similar size (Fig. 5A-C). This suggested the existence of bivalent promoter domains, which are known to be enriched in lineage-regulatory genes (Mikkelsen et al., 2007). Consistently, DE genes were more significantly associated with bivalent promoter domains at their TSS positions than randomly selected genes, regardless of their similar gene expression levels (Fig. 5D,E: left panels, white curve; Fisher's exact test, $P < 10^{-10}$). By

separating H3K4me3 (active and bivalent promoters) and H3K27me3 (bivalent promoters only) signals, it appeared that H3K4me3 active mark was overall less enriched at the TSS positions of DE genes than randomly selected genes (Fig. 5D,E: middle panels), whereas the H3K27me3 repressive mark displayed an opposite distribution (Fig. 5D,E: right panels). Although we cannot exclude that the increased ratio between repressive and active signal at promoters of genes affected by TF overexpression may reflect regulatory dynamics in the different cell populations (Hong et al., 2011), bivalent promoter domains suggest that DE genes are overall dynamically regulated and likely associated with CT differentiation and subtype-specific function, as opposed to housekeeping and ubiquitous genes that would be active and expressed across all cell types in limb cultures.

Genome-wide CT-associated TF occupancy indicates a common regulatory core and distinct functions

To further clarify the molecular mechanisms downstream of each TF, we aimed to investigate their genome-wide binding profile. ChIP-seq was performed in two independent biological replicates of 5-day chMM cultures overexpressing each of the TFs by using an antibody directed against the 3F tag (Fig. S1). Similarity across all ChIP-seq signal profiles was assessed genome-widely in 500-bp non-overlapping windows by PCA. Comparison of the three first principal components partitioned the TF signal profiles by biological replicates and TF subgroups (Fig. 6A), indicating that paralogous TFs (OSR1/OSR2 and KLF2/KLF4) had a similar distribution across the genome. Following peak calling, 95,884 TF binding sites (TFBS) were identified (OSR1, 20,983; OSR2, 22,403; EGR1, 16,627; KLF2, 21,352; and KLF4, 14,519), corresponding to ten times as many DE genes. To assess TFBS functionality, binding locations identified for each TF were intersected with the regulatory domains. We focused on TFBS contained within promoters and enhancers, since we considered that binding events

located in these regulatory domains likely contributed to the regulation of gene expression. Out of the 95,884 binding sites identified across all TFs, 31,289 (32.6%) overlapped promoter and enhancer regions, corresponding to 3,819-9,291 (17.9%-55.9%) binding events for each TF (Fig. 6B). *De novo* motif analysis was then performed on the 1,000 most significant binding sites for each TF. Recognition motifs identified for OSR1 and OSR2 were very similar and highly conserved with their known binding motifs in the fruit fly and the mouse (Fig. 6C) (Badis et al., 2009; Meng et al., 2005). In agreement with previous reports, EGR1 and KLF4 binding motifs were enriched in cytosine/guanine (Fig. 6C) (Badis et al., 2009; Chen et al., 2008). KLF2 recognition motif was highly consistent with the core binding sequence of the KLF protein family and was similar to the KLF4 secondary motif (Fig. 6C) (Sunadome et al., 2011). Both binding motifs identified for KLF4 could contribute to its regulatory pattern observed in limb cell cultures, considering the 767 DE genes specifically identified for KLF4 and the 1,866 DE genes shared between KLF4 and KLF2 (Fig. 3B).

Investigation of the genome-wide TF occupancy within promoters and enhancers revealed a consistency with the regulatory profiles retrieved from the RNA-seq data and the analogous recognition motifs. While 62.0% of binding regions were specific to a single TF, 38.0% were shared by at least two TFs and 5.9% were common to the five TFs (Fig. S7A: SuperExactTest for the 5-TFs occupancy, $P < 10^{-10}$). Closer investigation revealed that OSR1/OSR2 and EGR1/KLF4 tended to bind preferentially at similar regions (Fig. S7B-E: Fisher's exact test, $P < 10^{-8}$), whereas KLF2 did not display any preferential binding with any of the other TFs, including KLF4 (Fig. S7F). We hypothesized that the genome-wide binding of KLF4 was mainly influenced by its primary binding motif that resembles the EGR1 recognition motif (Fig. 6C). To further distinguish between indirectly and directly regulated genes, TFBS located within regulatory domains were intersected with the 4,298 DE genes identified from the RNA-seq data by investigating regions spanning from 10 kb upstream of the gene TSS to 10 kb downstream of the gene 3'-end. This resulted in the identification of 3,210 genes that were

potentially directly regulated by the TFs (Table S1). The proportion of putative direct targets ranged from 20.9% (OSR1, 417; KLF2, 449) to 49.4% (EGR1, 677), depending on the TF (Fig. 6D). Consistent with the previous observations that the TFs shared common regulatory patterns in addition to their own specificity, the 3,210 genes considered as potential direct targets corresponded to 1,858 non-redundant genes (Fig. 6E). While 1,076 (57.9%) genes were directly regulated by a single TF, 782 (42.1%) genes were shared by at least two TFs, including 77 (4.1%) genes common to all TFs (Fig. 6E: SuperExactTest for the 5-TFs direct targets, $P < 10^{-10}$). Consistent with their high number of shared target genes, OSR1/OSR2, EGR1/KLF4 and KLF2/KLF4 tended to occupy similar binding locations in the vicinity of their common target genes (Fig. S8: Fisher's exact test, $P < 10^{-4}$). Altogether, the binding profiles of CT-associated TFs reflect their specificity and similarity in regards to their regulatory patterns observed at the gene expression level.

Validation of selected target genes

Coexpression of a TF and its putative target gene is a prerequisite for transcriptional regulation. Therefore, we compared the expression domains of the TFs with that of selected candidate genes in chick limbs. *NTN1* (netrin 1) was one of the genes that was upregulated in limb cell cultures upon overexpression of each TF (Fig. 7A, Fig. S9A, Table S1), through binding within an intronic enhancer (Fig. 7B). *NTN1* encodes a laminin-related secreted protein involved in axon guidance (Dominici et al., 2017; Serafini et al., 1996). In E5.5 chick embryos, *NTN1* was expressed in both limb stylopod and zeugopod, displaying overlapping expression domains with those of all five TFs (Fig. 7C-H). At E8, *NTN1* was expressed in tendons, overlapping with *EGR1* expression domain close to muscle attachment (Fig. 7I,J). *NTN1*, *OSR1* and *OSR2* expression was observed in muscle CT at E9.5 (Fig. 7K-M'). In addition, *NTN1* transcripts

were detected in tissues delineating tendons at E9.5, similarly to *KLF2* and *KLF4* transcripts (Fig. 7N-P).

Given the similar regulatory profiles of OSR1 and OSR2, we also selected *WNT11*, a common target gene of both TFs. *WNT11* encodes a secreted component of the non-canonical Wnt planar cell polarity pathway (Gao, 2012), which is involved in regulating muscle fibre type and orientation (Anakwe et al., 2003; Gros et al., 2009). Both OSR factors increased *WNT11* expression in chMM cultures and bound at the same location within an intronic enhancer (Fig. 8A,B, Fig. S9B, Table S1). In E5.5 chick embryos, *WNT11* was expressed in limb mesenchyme, consistent with *OSR1* and *OSR2* expression patterns (Fig. S9C-E). At E8 and E9.5, *WNT11* transcripts were detected in irregular CT within and surrounding muscles, overlapping with *OSR1* and *OSR2* transcripts (Fig. 8D-I). An additional target gene, *GDF6*, which encodes a secreted signalling factor of the TGF-β superfamily (Settle et al., 2003), was upregulated upon overexpression of OSR1 and OSR2 in chMM cultures (Fig. 8A, Fig. S9B, Table S1). However, only a binding site for OSR2 was detected in the vicinity of *GDF6*, indicating that OSR1 was not directly involved in the regulation of *GDF6* expression (Fig. 8C). In limbs of E5.5 and E8 chick embryos, *GDF6* expression domains overlapped with those of *OSR2* (Fig. 8J-L, Fig. S9D,F). In addition to *OSR2* expression in muscle CT, we observed *OSR2* transcripts in limb myosin^{+} cells at E9.5 (Fig. 8H) (Nassari et al., 2018 preprint). Consistently, we identified *FHL1* (four and a half LIM domains 1) among the OSR2 direct target genes (Fig. S10A,B). *FHL1* was expressed in CT at E8 (Fig. S10C,D) and in both muscle CT and fibres at E9.5 (Fig. S10E,E'). Interestingly, mutations in *FHL1* are causative for various rare X-linked myopathies (e.g. Gueneau et al., 2009).

As a specific target gene of EGR1, we selected *WNT4*, which encodes a secreted member of the canonical Wnt signalling pathway (DiRocco et al., 2013). *WNT4* was upregulated upon EGR1 overexpression in chMM cultures and was associated with an EGR1 binding site in its

promoter region (Fig. 8M,N, Fig. S9G, Table S1). This is consistent with previous findings where EGR1 has been shown to bind upstream of *Wnt4* gene in the uterine endometrium during mouse pregnancy (Liang et al., 2014). *EGR1* and *WNT4* displayed overlapping expression domains in proximal regions of forelimbs of E5.5 chick embryos (Fig. S9H,I) and in tendons, close to muscle attachment, in E8 limbs (Fig. 8O-Q).

Given the common regulatory patterns of both KLF factors, we selected *FZD1*, which encodes a frizzled class receptor of Wnt signalling proteins (Laeremans et al., 2010). *FZD1* was upregulated upon overexpression of KLF2 and KLF4 in chMM cultures (Fig. 8R, Fig. S9J, Table S1) and harboured a binding site for both KLF factors within its promoter region (Fig. 8S). In E8 chick embryos, *FZD1* was expressed in tissues delineating tendons, overlapping with the expression domains of *KLF2* and *KLF4* (Fig. 8U-W'). Considering that KLF4 also displayed a distinct regulatory profile (Fig. 6E), we selected *INHBA*, which encodes the inhibin beta A subunit, a member of the TGF-β signalling pathway (Howley et al., 2016). *INHBA* was upregulated upon KLF4 overexpression in chMM cultures (Fig. 8R, Fig. S9J, Table S1). In addition, a KLF4 binding site was located within an enhancer upstream of the TSS position of *INHBA* (Fig. 8T). In chick limbs, *INHBA* and *KLF4* displayed overlapping expression domains at E5.5 and in tissues delineating tendons at E8 (Fig. 8V,V',X,X', Fig. S9K-M). Altogether, the selected target genes and their related CT-associated TFs exhibit overlapping expression domains in chick limbs.

Common and divergent signalling/ECM signatures regulated by the CT-associated TFs

It is generally assumed that CT cells shape their microenvironment mainly by production of signalling/ECM molecules and/or via remodelling of the ECM. To finally explore how this feature could be guided by the CT subtype-specific TFs, we built a regulatory network on the 189 DE genes that were associated with seven of the previously identified signalling pathways (Fig. 4A,B, Table S1). The resulting transcriptional network was composed of 513 interactions divided between 175 (34.1%) direct and 338 (65.9%) indirect connections (Fig. 9A). This network highlighted common and unique features for the CT-associated TFs. 38 (20.1%) genes were regulated by all five TFs, revealing a CT-typical signalling signature, whereas 47 (24.9%) genes were exclusively shared by paralogous TFs (OSR1/OSR2 and KLF2/KLF4) and 45 (23.8%) genes were specific to a single TF (Fig. 9A, Table S1). The regulatory network was then subdivided for each individual TF to visualize the molecular interplay of each TF on selected signalling pathways (Figs S11-S15). For instance, the Wnt signalling pathway was differently affected depending on the TF, with different sets of *WNT* ligand and *FZD* receptor genes regulated by each TF (Figs S11-S15).

To reduce complexity, we then focused on the Notch, TGF-β and Wnt signalling pathways (Fig. 9B). Key components of these signalling pathways, *NOTCH1* (Notch receptor) and *SMAD4* (TGF-β signalling transducing protein) were regulated by all five TFs (Fig. 9B, Table S1). By contrast, other genes were regulated by a subset of TFs. For instance, *WNT11* and *BMPR1B* (BMP receptor) were specific to OSR1 and OSR2, whereas *FZD1* and *PRKCQ* (protein kinase C theta) were regulated exclusively by both KLF factors (Fig. 9B, Table S1). Lastly, we found genes that were specific to a single TF. This is the case for *GDF6* and *SMAD9* directly upregulated by OSR2, *WNT4* and *TCF7L1* (*TCF3*) directly upregulated by EGR1, and *INHBA*

and *BMP8B* (BMP secreted ligand) directly upregulated by KLF4 (Fig. 9B, Table S1). Altogether, this regulatory network identifies signalling genes that likely contribute to the biological function of all CTs or CT subtypes.

By finally focusing on direct target genes associated with the ECM, we found that the TFs regulated distinct, nevertheless partly overlapping molecular ECM niches (Fig. 9C, Table S1). *ADAMTS15*, for example, was directly upregulated by the five TFs and *ADAMTS8* was specific to EGR1, whereas *ADAMTS18* was directly downregulated by OSR2 and KLF2 (Fig. 9C, Table S1). ADAMTS proteins are secreted metalloproteases with thrombospondin type-I motif that are involved in procollagen processing (Apte, 2009). While ADAMTS15 and ADAMTS8 have proteoglycanolytic activity (Apte, 2009), mutations in *ADAMTS18* have been associated with bone disorders (Wei et al., 2014). In addition, CT-associated TFs appeared to mediate collagen deposition by directly regulating genes encoding collagen α-chains. *COL4A1* and *COL4A2* were directly upregulated by OSR1, OSR2 and KLF2 (Fig. 9C, Table S1). Type-IV collagen contributes to the assembly of basal lamina by binding to laminins (Mouw et al., 2014). By contrast, *COL9A1*, *COL9A2* and *COL11A1* were directly downregulated by OSR1 and OSR2 (Fig. 9C, Table S1). Type-IX and XI collagens are known to form a network with type-II collagen in cartilaginous ECM (Fernandes et al., 2003). KLF4 directly promoted the expression of *COL1A1* (Fig. 9C, Table S1). Type-I collagen fibrils are the main component of tendons (Gaut and Duprez, 2016). The ECM also acts as a source of developmental signals by sequestering and diffusing paracrine factors. The TFs appeared to directly mediate the positive expression of genes encoding laminin-related secreted netrins, such as *NTN1* (all five TFs), *NTN3* (EGR1 and KLF4), *NTN4* (OSR1 and EGR1) and *NTNG1* (OSR2) (Fig. 9C, Table S1). In conclusion, the CT-associated TFs contribute to provide distinct local patterning cues by mediating the expression of specific environmental molecules.

Discussion

The transcriptional network downstream of five CT-associated zinc finger TFs presented here identifies common and specific molecular signatures involved in limb CT specification. TF overexpression led to transcriptional changes in limb cells impacting on numerous cellular processes, including cell-cell/cell-matrix adhesion, cell communication and migration. Consistently, genes encoding signalling molecules, ECM components and cytoskeletal proteins appeared as regulated by the five TFs.

Core molecular network downstream of the five TFs

Among the 4,298 non-redundant DE genes upon overexpression of the five TFs, 2,811 (65.4%) were shared by at least two TFs, while 726 (16.9%) were common to all TFs. When direct regulation as judged by TF binding was considered, 77 genes were shared between the five TFs. We note that we performed a conservative analysis and also restricted regulatory elements to a distance of 20 kb. It is well established that enhancer elements can be located further away, however identification of these regulatory interactions would include analysis of the 3D chromatin structure (de Laat and Duboule, 2013). Consequently, the number of common direct targets, which we identified is likely to be imperfect. Our data nevertheless show that the five TFs display common direct target genes despite their expression in different subcompartments of the limb musculoskeletal system. This indicates that irrespective of CT type, whether it is specialized, dense regular or dense irregular, key molecular features are shared during the differentiation process of CT types, suggesting an archetypical CT signature.

One example for a common and directly regulated gene downstream of the five TFs is *NTN1*. Netrin 1 is a secreted ligand involved in axon guidance and developmental angiogenesis, in addition to preventing apoptosis triggered by one of its receptors, DCC (deleted in colorectal cancer) (Cirulli and Yebra, 2007). With the exception of EGR1, which only activates the

expression of netrin ligands (*NTN1*, *NTN2* and *NTN3*), the other TFs positively regulate the expression of netrin receptors, *UNC5A* and/or *UNC5B* (Table S1), known to mediate netrin 1-induced axon chemorepulsion (Cirulli and Yebra, 2007). Our data suggests that NTN1 is an unexpected actor involved in migration and/or survival of CT cells during limb development.

Notably, the molecular core downstream of the five TFs comprises a myofibroblast signature with *SRF*, *TAGLN* (*SM22*, transgelin), *TAGLN2* (transgelin 2), *CNN1* (calponin 1) and *ACTG2* (actin gamma 2) genes, which are positively activated by the five TFs, although not involving systematically direct binding sites (Table S1). *SMAD4* is a well-known profibrotic factor downstream of TGF-β1 (Xu et al., 2016) and is directly regulated by all TFs (Table S1). The myofibroblast signature upon TF overexpression indicates that developmental CT differentiation shares molecular mechanisms with myofibroblast activation during fibrosis. We note that *NOTCH1*, a component of a developmental signalling pathway described to be also involved in adult fibrosis (Hu and Phan, 2016), is a common and directly regulated gene downstream of the five TFs (Table S1). The upregulation of Notch pathway components by each of the TFs suggests an unexpected involvement of Notch signalling in limb CT formation during development.

It has to be noted that none of the TFs investigated here is a comprehensive marker for the different CT subtypes. As example, muscle CT appears to be a heterogeneous entity with areas in the mouse limb specifically expressing OSR1, while other areas express TCF4 during development (Vallecillo-García et al., 2017). Consequently, the molecular network identified here may not uniformly apply to all muscle CT or tendon cells in the limb bud. Taking into consideration the common regulatory features exhibited by the five TFs, however, makes us confident that the mechanisms we identified by choosing five example TFs may be a common theme with foreseeable local variation.

Specific regulatory patterns downstream of the five TFs

In addition to sharing a common molecular core, each TF displayed a specific regulatory pattern, albeit convergence was observed between related TFs, i.e. between OSR1 and OSR2 associated with irregular CT, and between EGR1, KLF2 and KLF4 mainly associated with regular CT. OSR1 and OSR2 are two markers of irregular CT and overexpression of each factor promotes the expression of irregular CT markers, such as *COL3A1*, while inhibiting that of cartilage markers in chick limb cells, as previously observed (Stricker et al., 2012) and consistent with the upregulation of cartilage-associated genes observed in irregular CT cells of *Osr1* null mouse embryos (Vallecillo-García et al., 2017). The master regulator of cartilage *SOX9* appears to be a direct target of OSR2 and the secondary regulatory factors *SOX5* and *SOX6* appear to be direct targets of both OSR1 and OSR2 in chMM cultures (Table S1). OSR1 and OSR2 share 318 common target genes, but also display their own specificity. While only 42 target genes are unique to OSR1, 250 target genes are specifically regulated by OSR2 (Table S1). The BMP ligand *GDF6* is one of the OSR2 specific target genes. GDF6 is known to play a role in establishing boundaries between skeletal elements during limb development, since inactivation of the *Gdf6* gene causes defects in joint, ligament and cartilage formation in mice (Settle et al., 2003). This is in line with *Osr2*/*OSR2* expression in joint interzones in mouse (Stricker et al., 2006) and chick embryos (Fig. 8K), as well as with the joint fusion defects observed in *Osr1*/*Osr2* double mutant mice (Gao et al., 2011).

Although not being specific to tendons, EGR1 overexpression is sufficient to drive tendon cell differentiation in mouse mesenchymal stem cells (Guerquin et al., 2013). Over 100 genes upregulated upon EGR1 overexpression were listed as being enriched in the transcriptome of *Scx*$^{+}$ cells isolated from limbs of mouse embryos (Havis et al., 2014), including *ADAMTS8*, *ADAMTS15*, *TAGLN*, *TAGLN2*, *FZD5* and *WNT4*, among others (Table S1). *BMP4*, known to be expressed in chick limb tendons (Wang et al., 2010), was also positively regulated by EGR1

(although not directly) in our data (Table S1). EGR1 is characterised as a fibrosis-promoting factor in many organs (Ghosh et al., 2013). EGR1 has been also shown to directly regulate *Tgfb2* transcription in adult mouse tendons (Guerquin et al., 2013). We note that *TGFB1* is positively regulated by EGR1 (albeit not directly) in chick limb cells (Table S1).

The function of KLF2 and KLF4 in limb musculoskeletal system formation is currently not known. However, we show here that both KLFs display a striking expression delineating *SCX*$^{+}$ tendon/ligaments. In addition to the clear adhesion/migration signature downstream of both KLF factors in chick limb cells, KLF2 and KLF4 activate cell cycle genes such as *CDKN1A* (*P21*) and pluripotency-associated genes (*SOX7* and *DKK1*, among others) (Table S1). The recognized function of KLF2 and KLF4 in somatic cell reprogramming and pluripotency (Jiang et al., 2008) raises the interesting hypothesis that cells surrounding *SCX*$^{+}$ expression domains could be a source of tendon progenitors during development. Consistent with this idea, different tenogenic properties have been described for peritenon cells and tendon proper cells (Mienaltowski et al., 2014). Given the identified role of the Notch signalling pathway in cell stemness (Mourikis and Tajbakhsh, 2014), the upregulation of Notch signalling components upon overexpression of KLF2 and KLF4 also suggests this potential implication. Beyond the 313 target genes that are shared between both KLFs and their similar binding occupancy in the vicinity of these target genes, KLF4 possesses 439 specific target genes. KLF4 specificity is corroborated with its primary binding motif that differs from the KLF core binding sequence identified in KLF2 and KLF4 ChIP-seq data (Fig. 6C). Indeed, the KLF4 binding site identified upstream of *INHBA* encompasses its primary recognition motif, whereas KLF2 and secondary KLF4 binding motifs are detected in the promoter region of their common target gene *FZD1* (Fig. 8S,T).

A versatile molecular toolkit for shaping local niches

A significant proportion of directly or indirectly regulated DE genes comprises genes encoding signalling-associated molecules or ECM components and cell-matrix attachment molecules. The ECM is a three-dimensional insoluble network composed of secreted macromolecules, which provides positional and physical cues to influence cell position, migration and differentiation (Charras and Sahai, 2014; Mammoto et al., 2013; Rozario and DeSimone, 2010). Moreover, the ECM is a storage space for diverse growth factors that can be released upon e.g. proteolytic cleavage or mechanical stimulation. In this view, the ECM is both a scaffold structure and an integral part of cell-cell signalling mechanisms. Our data provide evidence that regional subspecification of limb bud mesenchymal tissues by TFs may be concomitant to local changes in the extracellular milieu. Of note, we show that there is a common ECM signature activated by the five CT-associated TFs in addition to specific ECM and signalling factor genes. Individual TF or combinatorial TFs will impinge on the production of a particular ECM with specific growth factor decoration. This is likely to influence the behaviour of neighbouring tissues and to create beneficial environments for invading cells. This is in line with the recognized importance of cell-ECM interactions for skeletal muscle, nerve and blood vessel development (Eichmann et al., 2005; Thorsteinsdóttir et al., 2011). Thus, coordinated expression of a combination of TFs may be an elegant and adaptable way to achieve tissue (sub)compartmentalization and to convey patterning information in development.

Concluding remarks

In conclusion, the transcriptional network presented here brings new insights into the molecular mechanisms orchestrating chick limb CT differentiation and function. The common and specific programs identified here are likely to be at the root of tissue subspecification and local compartmentalization in developing limbs leading to the creation of local niches supporting organogenesis. This regulatory network and the genome-wide data offer valuable resources and open new roads to better analyse and understand CT formation and function during limb development. In addition, such adaptable local transcriptional programs may apply to diverse contexts and might be a general principle of functional modulation.

Materials and Methods

Experimental procedures

Chick embryos

Fertilized eggs used for in situ hybridization were provided by the Institut de Sélection Animale (JA 57 strain, Lyon, France). Fertilized eggs used to prepare chMM cultures were obtained from VALO BioMedia (Lohmann Selected Leghorn strain, Osterholz-Scharmbeck, Germany). Embryos were staged according to the number of days in ovo at 37.5°C.

Molecular cloning of the transcription factors

The CDSs of the chicken TFs OSR1, OSR2, EGR1, KLF2 and KLF4 were amplified by PCR by using the primers listed in (Table S2). Cloning of the TF CDSs was performed by using a modified version of the pSlax-13 vector and the RCAS-BP(A) vector as previously described (Ibrahim et al., 2013), with the exception that the 3F tag was fused C-terminally to each CDS.

Chick micromass cultures

chMM cultures were prepared as previously described (Solursh et al., 1978). Briefly, limb buds were extracted from E4.5 chick embryos, ectoderm was dissociated by using a Dispase solution (Gibco) at 3 mg/mL, and limb mesenchyme was digested by using a solution composed of 0.1% Collagenase type Ia (Sigma-Aldrich), 0.1% Trypsin (Gibco) and 5% FBS (Biochrom) in 1X DPBS (Gibco). Prior to seeding, mesenchymal cells were mixed with retroviruses (1:1) and maintained in culture for 5 days at 37°C in DMEM/Ham's F-12 (1:1) medium (Biochrom) supplemented with 10% FBS, 0.2% chicken serum (Sigma-Aldrich), 1% L-glutamine (Lonza) and 1% penicillin/streptomycin (Lonza). To assess cartilage differentiation, chMM cultures were fixed for 30 min with Kahle's fixation solution (1% formalin, 30% ethanol and 4% acetic acid) and stained overnight at 4°C in 1% Alcian blue (Sigma-Aldrich) in 0.1 M HCl. Chondrogenic matrix areas were measured by using ImageJ (Schneider et al., 2012). For Eosin

staining, chMM cultures were fixed overnight with 4% PFA in 1X PBS at 4°C and incubated for 2 min with 2.5 g/L of Eosin (Sigma-Aldrich) in 80% ethanol and 0.5% acetic acid. Viral 3F-tagged TF expression was monitored by using a mouse antibody directed against the 3F tag (Sigma-Aldrich, F1804; 1:500). Immunohistological staining was performed by using the Vectastain Elite ABC and the DAB Peroxidase Substrate kits (Vector Laboratories).

RNA sequencing

Two biological replicates of chMM cultures were prepared from two independent pools of E4.5 limb buds and infected for 5 days with RCAS-BP(A) retroviruses overexpressing each of the TFs or no recombinant protein as control. For both replicates, RNA extracts were obtained by harvesting 6 chMM cultures with RLT buffer (Qiagen). Total RNAs were purified by using the RNeasy mini kit (Qiagen) in combination to a DNase I (Qiagen) treatment to prevent genomic DNA contamination. RNA libraries were prepared by using the TruSeq Stranded mRNA Library Preparation kit (Illumina), which enables to preserve the RNA strand orientation. Strand-specific 50-bp paired-end reads were generated by using a HiSeq 2500 sequencer (Illumina) with a mean insert size of 150 bp (Table S3).

ChIP sequencing

Harvesting of chMM cultures and ChIP experiments were performed as previously described (Ibrahim et al., 2013). Histone modification occupancy was investigated in two independent biological replicates of chMM cultures infected with RCAS-BP(A) retroviruses overexpressing no recombinant protein. 10 µg (8 chMM cultures) of chromatin extracts were incubated overnight at 4°C with gentle rocking with the following antibodies: 4 µg of mouse anti-H3K4me1 (Abcam, ab8895); 8 µL of mouse anti-H3K4me2 (Abcam, ab32356); 4 µL of mouse anti-H3K4me3 (Millipore, 07-473); 4 µg of mouse anti-H3K27ac (Abcam, ab4729); and 4 µg of mouse anti-H3K27me3 (Millipore, 07-449). TF binding profiles were investigated in two independent biological replicates of chMM cultures infected with RCAS-BP(A) retroviruses

overexpressing each of the TFs. 30 µg (24 chMM cultures) of chromatin extracts were incubated overnight at 4°C with gentle rocking with 10 µg of mouse anti-FLAG (Sigma-Aldrich, F1804). Antibody-TF/Histone-DNA complexes were pulled down by using 40 µL of magnetic beads (Dynabeads protein G, Thermo Fischer). Ethanol-precipitated ChIP samples were resuspended in 46 µL of ddH20. Libraries were prepared by using the NEBNext Ultra DNA Library Preparation kit for Illumina (New England Biolabs). 50-bp single-end reads were generated by using a HiSeq 1500 sequencer (Illumina) (Tables S4, S5). As input control, sonicated DNA from the nuclear fraction of each sample used for the ChIP procedures was also sequenced.

In situ hybridization

Endogenous expression of the TFs was assessed by in situ hybridization on paraffin-embedded tissue sections. Chick embryo limbs were fixed overnight at 4°C in 60% ethanol, 30% formaldehyde at 37% and 10% acetic acid, and further processed as previously described (Wilkinson et al., 1987). For whole-mount in situ hybridization, chick embryos were fixed overnight at 4°C with 4% formaldehyde in 1X PBS and processed as previously described (Henrique et al., 1995). The following probes were used: *cOSR1* and *cOSR2* (Stricker et al., 2006); *cEGR1* (Lejard et al., 2011); *cKLF2* and *cKLF4* (Antin et al., 2010). Expression of tendon and myogenic markers were assessed with the following probes: *cSCX* (Schweitzer et al., 2001); *cMYOD* (Pourquié et al., 1996). Primers listed in (Table S2) were used to generate probes detecting the following genes: *cFHL1*, *cFZD1*; *cGDF6*; *cINHBA*; *cNTN1* (Murakami et al., 2010); *cWNT4* (GEISHA ID, WNT4.UApcr); *cWNT11* (GEISHA ID, WNT11.UApcr).

Quantitative RT-PCR analysis

Total RNAs were isolated from independent biological replicates of chMM cultures infected for 5 days with RCAS-BP(A) retroviruses overexpressing each of the TFs or no recombinant protein as control. RNA extracts were obtained as described for RNA-seq. 500 ng of RNA extracts were used as template for cDNA synthesis using the High-Capacity cDNA Reverse Transcription kit (Applied Biosystems). Quantitative RT-PCR was performed by using the SYBR Green PCR Master mix (Applied Biosystems) in duplicates. Relative mRNA levels were calculated according to the 2-ΔΔCt method (Livak and Schmittgen, 2001). ΔCts were obtained from Ct normalized with chick *RPS17* (*S17*) and *GAPDH*. For each investigated gene, the mRNA levels of control chMM cultures were normalized to 1. Statistical analysis was performed by using Mann-Whitney U test with the GraphPad Prism V6 software. Primers used for quantitative RT-PCR are listed in (Table S2).

Computational analysis

Gene expression profiles

RNA-seq strand-specific read pairs were mapped against the chicken genome galGal4 (Hillier et al., 2004) by using TopHat2 v0.14 (Kim et al., 2013) (parameters: -r 150; -N 3; --read-edit-dist 3; --library-type fr-firststrand; -i 50; -G) and the gene annotation model previously generated (Orgeur et al., 2018). Alignment maps were split by strand by using SAMtools v1.2 (Li et al., 2009) according to their FLAG field (strand plus: -f 128 -F 16, -f 80; strand minus: -f 144, -f 64 -F 16). Fragments (both reads of a pair) mapped on gene features were counted by using featureCounts v1.4.6-p3 (Liao et al., 2014) (parameters: -p; -s 2; --ignoreDup; -B; -R). Chimeric fragments aligned on different chromosomes were taken into consideration to

overcome the gene fragmentation due to the location of gene parts on multiple chromosome contigs (Orgeur et al., 2018). Fragment counts were then normalized by using DESeq2 v1.8.1 (Love et al., 2014) and transcript abundances were calculated as transcripts per million (TPM) values according to the formula described in (Wagner et al., 2012). To evaluate the discrepancy among biological replicates and conditions, a regularized-logarithm (rlog) transformation was applied to normalized fragment counts followed by PCA analysis and hierarchical clustering of the Euclidean distances (Love et al., 2014). Differential expression analysis was finally carried out by using DESeq2 and a false-discovery rate (FDR, alpha) of 0.01. Genes with an absolute fold change of at least 2 and a Benjamini-Hochberg adjusted p-value (padj) below 0.01 were considered as being differentially expressed (Table S1). Heat maps were generated by using the function heatmap.2 from the R package gplots. For given gene lists, rlog transformed fragment counts were used as input and hierarchical clustering was performed according to the one minus Pearson correlation.

_K_-means gene clustering

K-means clustering was performed on the normalized fragment counts of the DE genes by using GENE-E (https://software.broadinstitute.org/GENE-E/) with a row distance metric set at 1 minus Pearson correlation and 2,000 iterations. The number of *K* clusters was defined at 8 because lower values did not separate distinct gene clusters and higher values subdivided meaningful gene clusters.

Gene ontology analysis

GO analyses were performed for given gene lists by using the PANTHER statistical overrepresentation test r20160321 (Mi et al., 2010) and the Bonferroni correction for multiple testing. The following annotations were interrogated: PANTHER version 10.0 released on 2015-05-15 for GO-slim biological process, cellular component and pathways; GO ontology database released on 2016-04-23 for GO biological process complete.

ChIP sequencing coverage profiles

50-bp single-end reads generated for each ChIP and input fractions were first filtered on their quality by using the FASTX-Toolkit v0.0.13 (http://hannonlab.cshl.edu/fastx_toolkit/). Reads with a median quality value of minimum 28 were retrieved and mapped against the chicken genome galGal4 (Hillier et al., 2004) by using BWA v0.5.9 (Li and Durbin, 2009) (default parameters). Uniquely mapped reads were then extracted and duplicated reads were finally removed by using the tool rmdup from SAMtools v1.2 (Li et al., 2009). Histone mark and TF coverage profiles were generated by using the tool bdgcmp from MACS2 v2.1.0.20140616 (Zhang et al., 2008). ChIP-seq signal was normalized independently for each biological replicate against the pooled input controls of both replicates according to the negative log10 of the Poisson p-value (-m ppois). Similarity between the TF binding profiles was assessed genome-widely in 500-bp non-overlapping windows by using PCA analysis with the R function prcomp (parameters: center TRUE; scale. TRUE).

Histone modification peak calling

Peak calling for the histone ChIP-seq was performed as suggested by the ENCODE consortium (Kellis et al., 2014). For each histone modification, peaks were called independently for each biological replicate and for the pooled biological replicates, each time against the merged input control of both replicates, by using MACS2 v2.1.0.20140616 (Zhang et al., 2008) (parameters: --bw 400, according to the sonicated DNA size; -g 1.0e9; --to-large). Except for the H3K27me3 mark, peak calling was performed twice for each replicate and pooled replicate: (i) narrow peaks passing a p-value (-p) of 0.01; and (ii) broad peaks passing an additional broad-peak p-value (-p 0.01; --broad; --broad-cutoff) of 0.1. Only broad peaks were called for the H3K27me3 ChIP-seq due to its diffused signal. Broad peaks detected for each replicate and pooled replicate that contain at least one narrow peak were extracted by using BEDtools intersect v2.24.0 (Quinlan and Hall, 2010). Final sets of peaks for each histone modification were obtained by filtering broad peaks called for the pooled replicates that are shared between both biological replicates independently.

Identification of regulatory domains

Regulatory domains were defined according to the combination of the different histone modification profiles obtained by ChIP-seq, independently of the gene annotation model and TSS positions given the fragmentation of the chicken genome (Orgeur et al., 2018). Domains were divided into three categories: (1) promoters; (2) enhancers; and (3) repression islands. (1) Promoters were defined according to the presence of H3K4me3 signal. (2) Enhancers corresponded to regions enriched for H3K4me1 and devoid of H3K4me3 signal. (3) Repression islands were distinguished by the unique presence of H3K27me3 signal. Additional regions enriched for H3K4me2 but with no detectable H3K4me1 signal were classified as promoters, whereas regions containing both H3K4me1/2 marks were defined as enhancers. Promoter and

enhancer domains were further subcategorised into four distinct states according to the active marks H3K4me3 and H3K27ac, and the repressive mark H3K27me3: (i) inactive, no active and repressive signal detected (H3K4me3^{-}, H3K27ac^{-}, H3K27me3^{-}); (ii) poised, no active mark but repressive signal detected (H3K4me3^{-}, H3K27ac^{-}, H3K27me3^{+}); (iii) active, only active mark detected (H3K4me3^{+} and/or H3K27ac^{+}, H3K27me3^{-}); and (iv) bivalent, both active and repressive marks detected (H3K4me3^{+} and/or H3K27ac^{+}, H3K27me3^{+}).

Chromatin landscape at TSS positions

Normalized ChIP-seq signal was averaged for each histone modification from -2.5 to +2.5 kb surrounding the TSS of all genes, DE genes and randomly selected genes. To further investigate the increased enrichment of H3K27me3 mark, the 4,298 DE genes were filtered based on three criteria: (i) gene located on one single chromosome with a minimum size of 20 kb; (ii) gene body length of at least 1 kb; and (iii) -10/+10-kb regions around TSS within the chromosome borders. The resulting list was composed of 3,070 DE genes. The same criteria were applied to the randomly selected genes giving rise to a set of 3,080 random genes. 10-kb regions surrounding each TSS were retrieved and split into 100 intervals of 200 bp. For the genes having multiple transcripts with distinct TSS positions, the most upstream TSS was selected. Regulatory domains contained in each 200-bp interval were recovered in order to identify the most dominant domain per interval. Intervals marked with active and bivalent promoters were plotted in blue and red, respectively.

Transcription factor peak calling

Quality of the TF ChIP-seq data was evaluated following the ENCODE consortium guidelines and metrics (Table S5) (Landt et al., 2012). Peaks were called by using MACS2 v2.1.0.20140616 (Zhang et al., 2008) with low-stringency parameters to obtain a significant list of peaks (--bw 130/135, as determined by the cross-correlation analysis; -g 1.0e9; --to-large; -p 0.025). Irreproducible discovery rate (IDR) analysis was performed on the top 125,000 peaks according to their p-value (Landt et al., 2012) (parameters: peak.half.width -1; min.overlap.ratio 0; is.broadpeak F; ranking.measure p.value). The final set of TFBS was determined by selecting the number of peaks with an IDR threshold below 0.01 obtained from the pooled-replicate consistency analysis.

Transcription factor occupancy

TFBS locations were intersected with regulatory domains and gene features by using BEDtools intersect v2.24.0 (Quinlan and Hall, 2010). Summits of TFBS located within promoters and enhancers were retrieved and extended ± 250 bp. Extended summits were then merged by using BEDtools merge v2.24.0 (Quinlan and Hall, 2010), resulting in a total of 17,714 binding regions. Merged regions bound by at least two different TFs were further investigated to measure the genome-wide shared occupancy level between each TF pair. For each TF, the number of binding locations that intersected each of the four remaining TFs were counted separately and compared to its total number of shared binding locations. A similar approach was applied when analysing the shared occupancy level of the TFs in the vicinity of their target genes, albeit only the binding locations of the TFs directly regulating them were considered.

Binding motif analysis

Motif analysis was performed by using DREME v4.11.2 (Bailey, 2011) (default parameters) on the 150-bp sequences surrounding the summits (± 75 bp) of the 1,000 most significant TF peaks that overlapped with promoters and enhancers. Recognition motifs thus identified were then compared against motif databases by using Tomtom v4.11.2 (Gupta et al., 2007) (default parameters). Given TF binding regions were scanned for the identified recognition motifs by using FIMO v4.12.0 (Grant et al., 2011) (default parameters).

Transcriptional regulatory network

The regulatory network was built on the 189 DE genes that were regulated by at least one TF and associated with the selected signalling pathways using Cytoscape v3.4.0 and the edge-weighted spring-embedded layout (Shannon et al., 2003). The five TFs were determined as source nodes, while the DE genes were defined as target nodes. Interactions between each source node and its target nodes were marked as direct or indirect whether the differential expression was associated with a functional TFBS or not, respectively.

Statistical analysis

Statistical significance was assessed by using the following R functions: (i) wilcox.test for Wilcoxon rank-sum test; (ii) fisher.test for Fisher's exact test; and (iii) supertest from the SuperExactTest package for multiset intersection test (Wang et al., 2015).

Acknowledgments

We are grateful to Stefan Mundlos (Charité Universitätsmedizin and Max Planck Institute for Molecular Genetics, Berlin, Germany) for generously sharing resources. We are thankful to the Sequencing Core Facility of the Max Planck Institute for Molecular Genetics for processing the RNA-seq. We are thankful to the Next Generation Sequencing Core Unit of the Berlin-Brandenburg Center for Regenerative Therapies for processing the ChIP-seq. We thank Peter Hansen and Peter N. Robinson (Charité Universitätsmedizin, BCRT, Berlin, Germany), as well as Marius van den Beek and Christophe Antoniewski (Institut de Biologie Paris-Seine, ARTbio, Paris, France) for providing access to Galaxy web servers. We thank Sophie Gournet (Institut de Biologie Paris-Seine, Paris, France) for illustrations.

Competing interests

The authors have declared that no competing interests exist.

Funding

This work was funded by the Deutsche Forschungsgemeinschaft (DFG; grant GK1631), the Université Franco-Allemande (UFA/DFH; grants CDFA-06-11 and CT-24-16), the Association Française contre les Myopathies (AFM; grants 16826 and 18626), the Fondation pour la Recherche Médicale (FRM; grant DEQ20140329500), the INSERM and the CNRS. MO and SN were part of the MyoGrad International Research Training Group for Myology. MO received financial support from the FRM (grant FDT20150532272) and SN received financial support from the AFM (grant 20150532272).

Data Availability

ChIP-seq and RNA-seq data have been deposited on the Gene Expression Omnibus (GEO) database under the SuperSeries accession number GSE100517.

Author contributions

Conceptualization: M.O., D.D., S.S.; Methodology: M.O., S.T.B., B.T., J.H., D.D., S.S.; Investigation: M.O., M.M., G.L., S.N., M.A.B.; Resources: B.T., J.H., D.D., S.S.; Formal analysis: M.O.; Validation: M.O., D.D., S.S.; Data curation: M.O.; Visualization: M.O., D.D., S.S.; Supervision: D.D., S.S.; Project administration: D.D., S.S.; Funding acquisition: M.O., S.N., D.D., S.S.; Writing - original draft: M.O., D.D., S.S.; Writing - review & editing: M.O., M.M., G.L., S.N., M.A.B., S.T.B., B.T., J.H., D.D., S.S.

References

Ahrens, P. B., Solursh, M., Reiter, R. S. and Singley, C. T. (1979). Position-related capacity for differentiation of limb mesenchyme in cell culture. *Dev. Biol.* **69**, 436–450.

Anakwe, K., Robson, L., Hadley, J., Buxton, P., Church, V., Allen, S., Hartmann, C., Harfe, B., Nohno, T., Brown, A. M. C., et al. (2003). Wnt signalling regulates myogenic differentiation in the developing avian wing. *Development* **130**, 3503–3514.

Antin, P. B., Pier, M., Sesepasara, T., Yatskievych, T. A. and Darnell, D. K. (2010). Embryonic expression of the chicken Krüppel-like (KLF) transcription factor gene family. *Dev. Dyn.* **239**, 1879–1887.

Apte, S. S. (2009). A disintegrin-like and metalloprotease (reprolysin-type) with thrombospondin type 1 motif (ADAMTS) superfamily: functions and mechanisms. *J. Biol. Chem.* **284**, 31493–31497.

Badis, G., Berger, M. F., Philippakis, A. A., Talukder, S., Gehrke, A. R., Jaeger, S. A., Chan, E. T., Metzler, G., Vedenko, A., Chen, X., et al. (2009). Diversity and complexity in DNA recognition by transcription factors. *Science* **324**, 1720–1723.

Bailey, T. L. (2011). DREME: motif discovery in transcription factor ChIP-seq data. *Bioinformatics* **27**, 1653–1659.

Braun, T. and Gautel, M. (2011). Transcriptional mechanisms regulating skeletal muscle differentiation, growth and homeostasis. *Nat. Rev. Mol. Cell Biol.* **12**, 349–361.

Charras, G. and Sahai, E. (2014). Physical influences of the extracellular environment on cell migration. *Nat. Rev. Mol. Cell Biol.* **15**, 813–824.

Chen, X., Xu, H., Yuan, P., Fang, F., Huss, M., Vega, V. B., Wong, E., Orlov, Y. L., Zhang, W., Jiang, J., et al. (2008). Integration of external signaling pathways with the core transcriptional network in embryonic stem cells. *Cell* **133**, 1106–1117.

Chevallier, A., Kieny, M. and Mauger, A. (1977). Limb-somite relationship: origin of the limb musculature. *J. Embryol. Exp. Morphol.* **41**, 245–258.

Christ, B., Jacob, H. J. and Jacob, M. (1977). Experimental analysis of the origin of the wing musculature in avian embryos. *Anat. Embryol. (Berl).* **150**, 171–186.

Cirulli, V. and Yebra, M. (2007). Netrins: beyond the brain. *Nat. Rev. Mol. Cell Biol.* **8**, 296–306.

de Laat, W. and Duboule, D. (2013). Topology of mammalian developmental enhancers and their regulatory landscapes. *Nature* **502**, 499–506.

DiRocco, D. P., Kobayashi, A., Taketo, M. M., McMahon, A. P. and Humphreys, B. D. (2013). Wnt4/β-catenin signaling in medullary kidney myofibroblasts. *J. Am. Soc. Nephrol.* **24**, 1399–1412.

Dominici, C., Moreno-Bravo, J. A., Puiggros, S. R., Rappeneau, Q., Rama, N., Vieugue, P., Bernet, A., Mehlen, P. and Chédotal, A. (2017). Floor-plate-derived netrin-1 is dispensable for commissural axon guidance. *Nature* **545**, 350–354.

Eichmann, A., Le Noble, F., Autiero, M. and Carmeliet, P. (2005). Guidance of vascular and neural network formation. *Curr. Opin. Neurobiol.* **15**, 108–115.

Fernandes, R. J., Schmid, T. M. and Eyre, D. R. (2003). Assembly of collagen types II, IX and XI into nascent hetero-fibrils by a rat chondrocyte cell line. *Eur. J. Biochem.* **270**, 3243–3250.

Gao, B. (2012). Wnt regulation of planar cell polarity (PCP). *Curr. Top. Dev. Biol.* **101**, 263–295.

Gao, Y., Lan, Y., Liu, H. and Jiang, R. (2011). The zinc finger transcription factors Osr1 and Osr2 control synovial joint formation. *Dev. Biol.* **352**, 83–91.

Gaut, L. and Duprez, D. (2016). Tendon development and diseases. *Wiley Interdiscip. Rev.*

Dev. Biol. **5**, 5–23.

Ghosh, A. K., Quaggin, S. E. and Vaughan, D. E. (2013). Molecular basis of organ fibrosis: potential therapeutic approaches. *Exp. Biol. Med.* **238**, 461–481.

Grant, C. E., Bailey, T. L. and Noble, W. S. (2011). FIMO: scanning for occurrences of a given motif. *Bioinformatics* **27**, 1017–1018.

Gros, J., Serralbo, O. and Marcelle, C. (2009). WNT11 acts as a directional cue to organize the elongation of early muscle fibres. *Nature* **457**, 589–593.

Gueneau, L., Bertrand, A. T., Jais, J.-P., Salih, M. A., Stojkovic, T., Wehnert, M., Hoeltzenbein, M., Spuler, S., Saitoh, S., Verschueren, A., et al. (2009). Mutations of the *FHL1* gene cause Emery-Dreifuss muscular dystrophy. *Am. J. Hum. Genet.* **85**, 338–353.

Guerquin, M.-J., Charvet, B., Nourissat, G., Havis, E., Ronsin, O., Bonnin, M.-A., Ruggiu, M., Olivera-Martinez, I., Robert, N., Lu, Y., et al. (2013). Transcription factor EGR1 directs tendon differentiation and promotes tendon repair. *J. Clin. Invest.* **123**, 3564–3576.

Gupta, S., Stamatoyannopoulos, J. A., Bailey, T. L., Noble, W., Maniatis, T., Goodbourn, S., Fischer, J., Pawson, T., Nash, P., Tompa, M., et al. (2007). Quantifying similarity between motifs. *Genome Biol.* **8**, R24.

Hasson, P. (2011). “Soft” tissue patterning: muscles and tendons of the limb take their form. *Dev. Dyn.* **240**, 1100–1107.

Hasson, P., DeLaurier, A., Bennett, M., Grigorieva, E., Naiche, L. A., Papaioannou, V. E., Mohun, T. J. and Logan, M. P. O. (2010). Tbx4 and Tbx5 acting in connective tissue are required for limb muscle and tendon patterning. *Dev. Cell* **18**, 148–156.

Havis, E., Bonnin, M.-A., Olivera-Martinez, I., Nazaret, N., Ruggiu, M., Weibel, J., Durand, C., Guerquin, M.-J., Bonod-Bidaud, C., Ruggiero, F., et al. (2014).

Transcriptomic analysis of mouse limb tendon cells during development. *Development* **141**, 3683–3696.

Heinz, S., Romanoski, C. E., Benner, C. and Glass, C. K. (2015). The selection and function of cell type-specific enhancers. *Nat Rev Mol Cell Biol* **16**, 144–154.

Henrique, D., Adam, J., Myat, A., Chitnis, A., Lewis, J. and Ish-Horowicz, D. (1995). Expression of a Delta homologue in prospective neurons in the chick. *Nature* **375**, 787–790.

Hillier, L. W., Miller, W., Birney, E., Warren, W., Hardison, R. C., Ponting, C. P., Bork, P., Burt, D. W., Groenen, M. A. M., Delany, M. E., et al. (2004). Sequence and comparative analysis of the chicken genome provide unique perspectives on vertebrate evolution. *Nature* **432**, 695–716.

Hong, S. H., Rampalli, S., Lee, J. B., McNicol, J., Collins, T., Draper, J. S. and Bhatia, M. (2011). Cell fate potential of human pluripotent stem cells is encoded by histone modifications. *Cell Stem Cell* **9**, 24–36.

Howley, B. V, Hussey, G. S., Link, L. A. and Howe, P. H. (2016). Translational regulation of inhibin βA by TGFβ via the RNA-binding protein hnRNP E1 enhances the invasiveness of epithelial-to-mesenchymal transitioned cells. *Oncogene* **35**, 1725–1735.

Hu, B. and Phan, S. H. (2016). Notch in fibrosis and as a target of anti-fibrotic therapy. *Pharmacol. Res.* **108**, 57–64.

Huang, A. H., Lu, H. H. and Schweitzer, R. (2015). Molecular regulation of tendon cell fate during development. *J. Orthop. Res.* **33**, 800–812.

Ibrahim, D. M., Hansen, P., Rödelsperger, C., Stiege, A. C., Doelken, S. C., Horn, D., Jäger, M., Janetzki, C., Krawitz, P., Leschik, G., et al. (2013). Distinct global shifts in genomic binding profiles of limb malformation-associated *HOXD13* mutations. *Genome*

Res. **23**, 2091–2102.

Jiang, J., Chan, Y. S., Loh, Y. H., Cai, J., Tong, G. Q., Lim, C. A., Robson, P., Zhong, S. and Ng, H. H. (2008). A core Klf circuitry regulates self-renewal of embryonic stem cells. *Nat. Cell Biol.* **10**, 353–360.

Kalluri, R. (2016). The biology and function of fibroblasts in cancer. *Nat. Rev. Cancer* **16**, 582–598.

Kardon, G. (1998). Muscle and tendon morphogenesis in the avian hind limb. *Development* **125**, 4019–4032.

Kardon, G., Harfe, B. D. and Tabin, C. J. (2003). A Tcf4-positive mesodermal population provides a prepattern for vertebrate limb muscle patterning. *Dev. Cell* **5**, 937–944.

Kellis, M., Wold, B., Snyder, M. P., Bernstein, B. E., Kundaje, A., Marinov, G. K., Ward, L. D., Birney, E., Crawford, G. E., Dekker, J., et al. (2014). Defining functional DNA elements in the human genome. *Proc. Natl. Acad. Sci. U. S. A.* **111**, 6131–6138.

Kim, T. K. and Shiekhattar, R. (2015). Architectural and functional commonalities between enhancers and promoters. *Cell* **162**, 948–959.

Kim, D., Pertea, G., Trapnell, C., Pimentel, H., Kelley, R. and Salzberg, S. L. (2013). TopHat2: accurate alignment of transcriptomes in the presence of insertions, deletions and gene fusions. *Genome Biol.* **14**, R36.

Kronenberg, H. M. (2003). Developmental regulation of the growth plate. *Nature* **423**, 332–336.

Laeremans, H., Rensen, S. S., Ottenheijm, H. C. J., Smits, J. F. M. and Blankesteijn, W. M. (2010). Wnt/frizzled signalling modulates the migration and differentiation of immortalized cardiac fibroblasts. *Cardiovasc. Res.* **87**, 514–523.

Lance-Jones, C. and Dias, M. (1991). The influence of presumptive limb connective tissue on

motoneuron axon guidance. *Dev. Biol.* **143**, 93–110.

Landt, S. G., Marinov, G. K., Kundaje, A., Kheradpour, P., Pauli, F., Batzoglou, S., Bernstein, B. E., Bickel, P., Brown, J. B., Cayting, P., et al. (2012). ChIP-seq guidelines and practices of the ENCODE and modENCODE consortia. *Genome Res.* **22**, 1813–1831.

Lejard, V., Blais, F., Guerquin, M.-J., Bonnet, A., Bonnin, M.-A., Havis, E., Malbouyres, M., Bidaud, C. B., Maro, G., Gilardi-Hebenstreit, P., et al. (2011). EGR1 and EGR2 involvement in vertebrate tendon differentiation. *J. Biol. Chem.* **286**, 5855–5867.

Li, H. and Durbin, R. (2009). Fast and accurate short read alignment with Burrows-Wheeler transform. *Bioinformatics* **25**, 1754–1760.

Li, H., Handsaker, B., Wysoker, A., Fennell, T., Ruan, J., Homer, N., Marth, G., Abecasis, G., Durbin, R. and 1000 Genome Project Data Processing Subgroup (2009). The Sequence Alignment/Map format and SAMtools. *Bioinformatics* **25**, 2078–2079.

Liang, X. H., Deng, W. B., Li, M., Zhao, Z. A., Wang, T. S., Feng, X. H., Cao, Y. J., Duan, E. K. and Yang, Z. M. (2014). Egr1 protein acts downstream of estrogen-leukemia inhibitory factor (LIF)-STAT3 pathway and plays a role during implantation through targeting Wnt4. *J. Biol. Chem.* **289**, 23534–23545.

Liao, Y., Smyth, G. K. and Shi, W. (2014). featureCounts: an efficient general purpose program for assigning sequence reads to genomic features. *Bioinformatics* **30**, 923–930.

Livak, K. J. and Schmittgen, T. D. (2001). Analysis of relative gene expression data using real-time quantitative PCR and the 2(-Delta Delta C(T)) Method. *Methods* **25**, 402–408.

Love, M. I., Huber, W. and Anders, S. (2014). Moderated estimation of fold change and dispersion for RNA-seq data with DESeq2. *Genome Biol.* **15**, 550.

Mammoto, T., Mammoto, A. and Ingber, D. E. (2013). Mechanobiology and developmental control. *Annu. Rev. Cell Dev. Biol.* **29**, 27–61.

Mathew, S. J., Hansen, J. M., Merrell, A. J., Murphy, M. M., Lawson, J. A., Hutcheson, D. A., Hansen, M. S., Angus-Hill, M. and Kardon, G. (2011). Connective tissue fibroblasts and Tcf4 regulate myogenesis. *Development* **138**, 371–384.

Meng, X., Brodsky, M. H. and Wolfe, S. A. (2005). A bacterial one-hybrid system for determining the DNA-binding specificity of transcription factors. *Nat. Biotechnol.* **23**, 988–994.

Mi, H., Dong, Q., Muruganujan, A., Gaudet, P., Lewis, S. and Thomas, P. D. (2010). PANTHER version 7: improved phylogenetic trees, orthologs and collaboration with the Gene Ontology Consortium. *Nucleic Acids Res.* **38**, D204-210.

Michaud, J. L., Lapointe, F. and Le Douarin, N. M. (1997). The dorsoventral polarity of the presumptive limb is determined by signals produced by the somites and by the lateral somatopleure. *Development* **124**, 1453–1463.

Mienaltowski, M. J., Adams, S. M. and Birk, D. E. (2014). Tendon proper- and peritenon-derived progenitor cells have unique tenogenic properties. *Stem Cell Res. Ther.* **5**, 86.

Mikkelsen, T. S., Ku, M., Jaffe, D. B., Issac, B., Lieberman, E., Giannoukos, G., Alvarez, P., Brockman, W., Kim, T.-K., Koche, R. P., et al. (2007). Genome-wide maps of chromatin state in pluripotent and lineage-committed cells. *Nature* **448**, 553–560.

Mourikis, P. and Tajbakhsh, S. (2014). Distinct contextual roles for Notch signalling in skeletal muscle stem cells. *BMC Dev. Biol.* **14**, 2.

Mouw, J. K., Ou, G. and Weaver, V. M. (2014). Extracellular matrix assembly: a multiscale deconstruction. *Nat. Rev. Mol. Cell Biol.* **15**, 771–785.

Murakami, S., Ohki-Hamazaki, H., Watanabe, K., Ikenaka, K. and Ono, K. (2010). Netrin 1 provides a chemoattractive cue for the ventral migration of GnRH neurons in the chick forebrain. *J. Comp. Neurol.* **518**, 2019–2034.

Murchison, N. D., Price, B. A., Conner, D. A., Keene, D. R., Olson, E. N., Tabin, C. J. and Schweitzer, R. (2007). Regulation of tendon differentiation by scleraxis distinguishes force-transmitting tendons from muscle-anchoring tendons. *Development* **134**, 2697–2708.

Nassari, S., Duprez, D. and Fournier-Thibault, C. (2017a). Non-myogenic contribution to muscle development and homeostasis: the role of connective tissues. *Front. Cell Dev. Biol.* **5**, 22.

Nassari, S., Blavet, C., Bonnin, M.-A., Stricker, S., Duprez, D. and Fournier-Thibault, C. (2017b). The chemokines CXCL12 and CXCL14 differentially regulate connective tissue markers during limb development. *Sci. Rep.* **7**, 17279.

Nassari, S., Orgeur, M., Blavet, C., Stricker, S., Fournier-Thibault, C. and Duprez, D. (2018). In addition to being a marker for muscle connective tissue, *Odd skipped-related 2* (*OSR2*) is expressed in differentiated muscle cells during chick development. *bioRxiv* doi:10.1101/255851.

Orgeur, M., Martens, M., Börno, S. T., Timmermann, B., Duprez, D. and Stricker, S. (2018). A dual transcript-discovery approach to improve the delimitation of gene features from RNA-seq data in the chicken model. *Biol. Open* **7**, bio028498.

Pourquié, O., Fan, C. M., Coltey, M., Hirsinger, E., Watanabe, Y., Bréant, C., Francis-West, P., Brickell, P., Tessier-Lavigne, M. and Le Douarin, N. M. (1996). Lateral and axial signals involved in avian somite patterning: a role for BMP4. *Cell* **84**, 461–471.

Quinlan, A. R. and Hall, I. M. (2010). BEDTools: a flexible suite of utilities for comparing genomic features. *Bioinformatics* **26**, 841–842.

Rozario, T. and DeSimone, D. W. (2010). The extracellular matrix in development and morphogenesis: a dynamic view. *Dev. Biol.* **341**, 126–140.

Schneider, C. A., Rasband, W. S. and Eliceiri, K. W. (2012). NIH Image to ImageJ: 25 years of image analysis. *Nat. Methods* **9**, 671–675.

Schweitzer, R., Chyung, J. H., Murtaugh, L. C., Brent, A. E., Rosen, V., Olson, E. N., Lassar, A. and Tabin, C. J. (2001). Analysis of the tendon cell fate using Scleraxis, a specific marker for tendons and ligaments. *Development* **128**, 3855–3866.

Serafini, T., Colamarino, S. A., Leonardo, E. D., Wang, H., Beddington, R., Skarnes, W. C. and Tessier-Lavigne, M. (1996). Netrin-1 is required for commissural axon guidance in the developing vertebrate nervous system. *Cell* **87**, 1001–1014.

Settle, S. H., Rountree, R. B., Sinha, A., Thacker, A., Higgins, K. and Kingsley, D. M. (2003). Multiple joint and skeletal patterning defects caused by single and double mutations in the mouse Gdf6 and Gdf5 genes. *Dev. Biol.* **254**, 116–130.

Shannon, P., Markiel, A., Ozier, O., Baliga, N. S., Wang, J. T., Ramage, D., Amin, N., Schwikowski, B. and Ideker, T. (2003). Cytoscape: a software environment for integrated models of biomolecular interaction networks. *Genome Res.* **13**, 2498–2504.

Solursh, M., Ahrens, P. B. and Reiter, R. S. (1978). A tissue culture analysis of the steps in limb chondrogenesis. *In Vitro* **14**, 51–61.

Spitz, F. and Furlong, E. E. M. (2012). Transcription factors: from enhancer binding to developmental control. *Nat. Rev. Genet.* **13**, 613–626.

Stricker, S., Brieske, N., Haupt, J. and Mundlos, S. (2006). Comparative expression pattern of Odd-skipped related genes Osr1 and Osr2 in chick embryonic development. *Gene Expr. Patterns* **6**, 826–834.

Stricker, S., Mathia, S., Haupt, J., Seemann, P., Meier, J. and Mundlos, S. (2012). Odd-skipped related genes regulate differentiation of embryonic limb mesenchyme and bone marrow mesenchymal stromal cells. *Stem Cells Dev.* **21**, 623–633.

Sunadome, K., Yamamoto, T., Ebisuya, M., Kondoh, K., Sehara-Fujisawa, A. and Nishida, E. (2011). ERK5 regulates muscle cell fusion through Klf transcription factors. *Dev. Cell* **20**, 192–205.

Thorsteinsdóttir, S., Deries, M., Cachaço, A. S. and Bajanca, F. (2011). The extracellular matrix dimension of skeletal muscle development. *Dev. Biol.* **354**, 191–207.

Vallecillo-García, P., Orgeur, M., Vom Hofe-Schneider, S., Stumm, J., Kappert, V., Ibrahim, D. M., Börno, S. T., Hayashi, S., Relaix, F., Hildebrandt, K., et al. (2017). Odd skipped-related 1 identifies a population of embryonic fibro-adipogenic progenitors regulating myogenesis during limb development. *Nat. Commun.* **8**, 1218.

Wagner, G. P., Kin, K. and Lynch, V. J. (2012). Measurement of mRNA abundance using RNA-seq data: RPKM measure is inconsistent among samples. *Theory Biosci.* **131**, 281–285.

Wang, H., Noulet, F., Edom-Vovard, F., Le Grand, F. and Duprez, D. (2010). Bmp signaling at the tips of skeletal muscles regulates the number of fetal muscle progenitors and satellite cells during development. *Dev. Cell* **18**, 643–654.

Wang, M., Zhao, Y. and Zhang, B. (2015). Efficient test and visualization of multi-set intersections. *Sci. Rep.* **5**, 16923.

Wei, J., Liu, C. and Li, Z. (2014). ADAMTS-18: a metalloproteinase with multiple functions. *Front. Biosci. (Landmark Ed.)* **19**, 1456–1467.

Wilkinson, D. G., Bailes, J. A., Champion, J. E. and McMahon, A. P. (1987). A molecular analysis of mouse development from 8 to 10 days post coitum detects changes only in embryonic globin expression. *Development* **99**, 493–500.

Xu, F., Liu, C., Zhou, D. and Zhang, L. (2016). TGF-β/SMAD pathway and its regulation in hepatic fibrosis. *J. Histochem. Cytochem.* **64**, 157–167.

Zhang, Y., Liu, T., Meyer, C. A., Eeckhoute, J., Johnson, D. S., Bernstein, B. E., Nussbaum, C., Myers, R. M., Brown, M., Li, W., et al. (2008). Model-based analysis of ChIP-Seq (MACS). *Genome Biol.* **9**, R137.

Figures

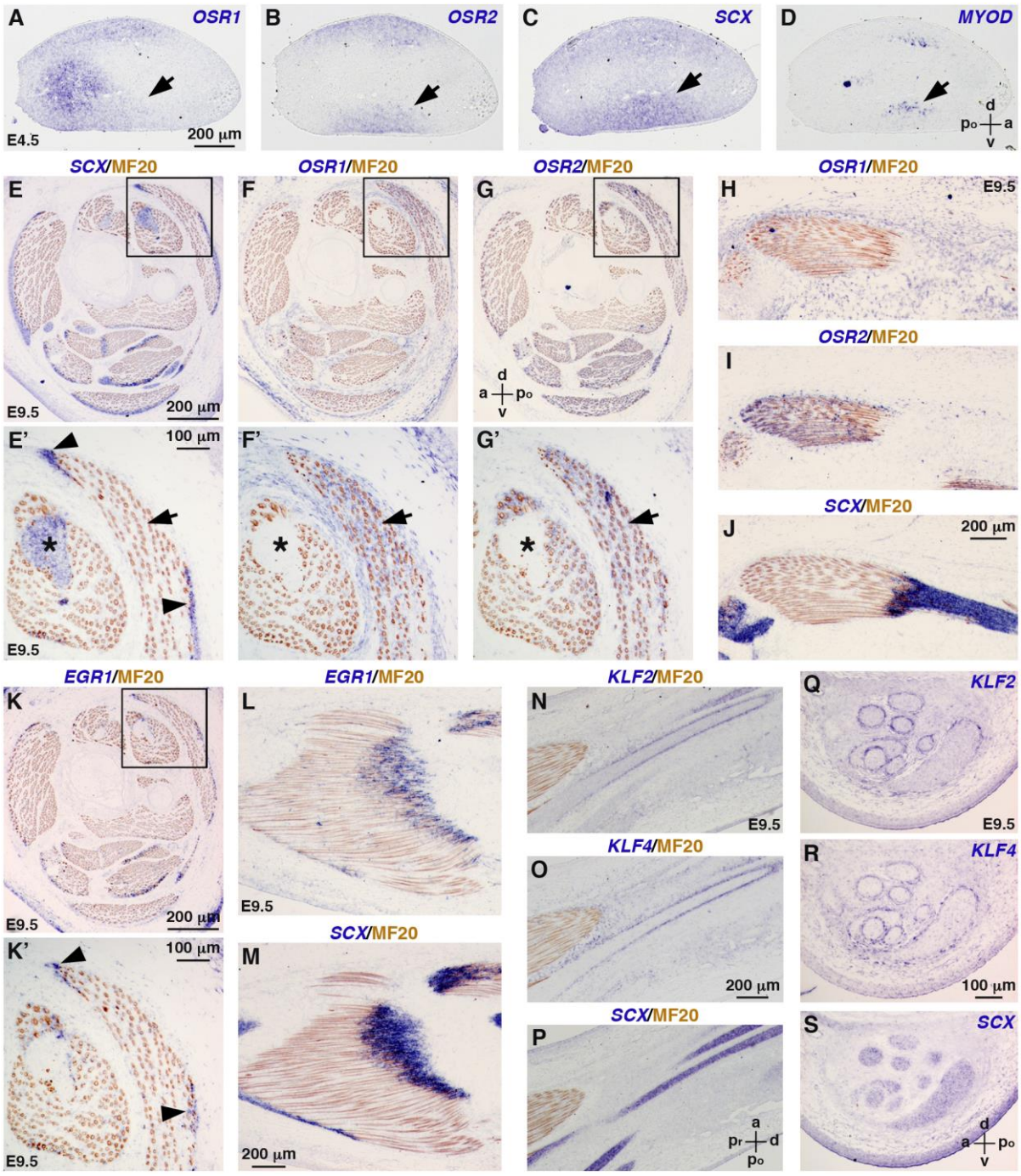

Fig. 1. Endogenous expression of CT-associated TFs in hindlimbs of chick embryos. (A-D) In situ hybridization to hindlimbs of E4.5 chick embryos. Adjacent and transverse limb sections were hybridized with *OSR1* (A), *OSR2* (B), *SCX* (C) and *MYOD* (D) probes (blue). Areas of overlapping expression are indicated by arrows. (E-S) In situ hybridization to

hindlimbs of E9.5 chick embryos followed by immunohistochemistry with the MF20 antibody (brown), which recognizes skeletal muscle myosins. (E-G',K,K') Adjacent and transverse limb sections were hybridized with *SCX* (E,E'), *OSR1* (F,F'), *OSR2* (G,G') and EGR1 (K,K') probes (blue). (E',F',G',K') are higher magnifications of the boxed areas in (E,F,G,K), respectively. Arrows indicate *OSR1* and *OSR2* overlapping expression domains that are exclusive to *SCX* expression domains (asterisks). Arrowheads indicate *EGR1* and *SCX* overlapping expression domains. (H-J) Adjacent and longitudinal limb sections were hybridized with *OSR1* (H), *OSR2* (I) and *SCX* (J) probes (blue). (L,M) Adjacent and longitudinal limb sections were hybridized with *EGR1* (L) and *SCX* (M) probes (blue). (N-S) Adjacent and longitudinal (N-P) or transverse (Q-S) limb sections were hybridized with *KLF2* (N,Q), *KLF4* (O,R) and *SCX* (P,S) probes (blue). pr, proximal; d, distal; a, anterior; po, posterior; d, dorsal; v, ventral.

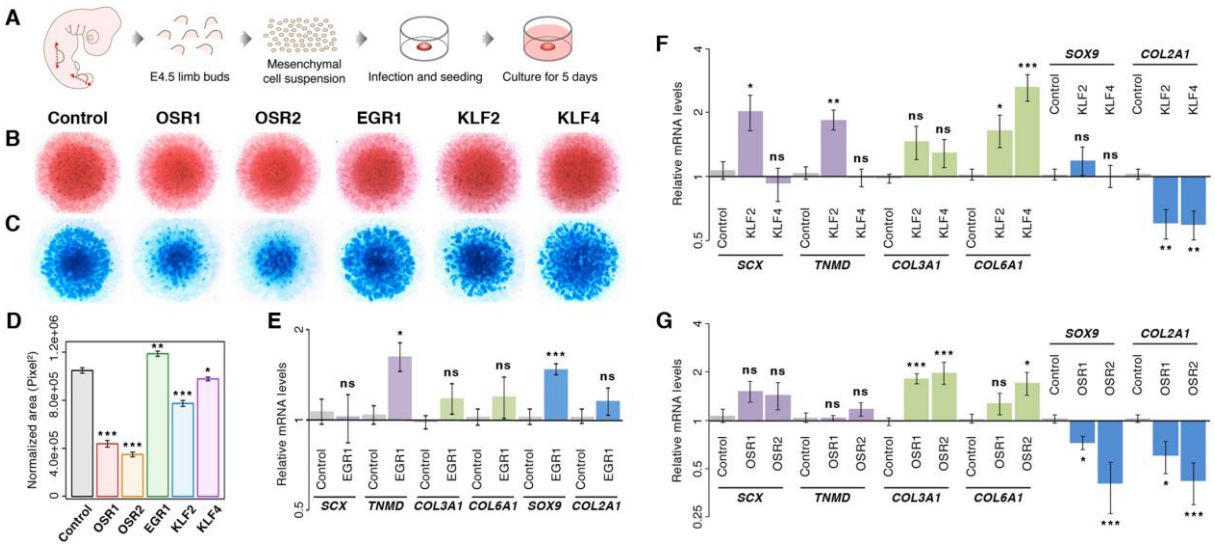

Fig. 2. Differentiation of limb mesenchymal cells following TF overexpression. (A) Chick mesenchymal cells were isolated from E4.5 limb buds and cultured in high density for five days. (B) Eosin staining of TF-overexpressing chMM cultures. (C) Alcian blue staining of cartilage nodules formed in TF-overexpressing chMM cultures. (D) Quantification of chondrogenic matrix production: mean ± SEM; paired Student's *t*-test: *, $P < 0.05$; **, $P < 0.01$; ***, $P < 0.001$. (E-G) Quantitative RT-PCR analysis of CT marker gene expression upon overexpression of EGR1 (E), KLF2/KLF4 (F) and OSR1/OSR2 (G) in chMM cultures. Graphs depict relative mRNA levels of *SCX* and *TNMD* (tendon markers), *COL3A1* and *COL6A1* (irregular CT markers), and *SOX9* and *COL2A1* (cartilage markers): mean ± SEM; two-tailed Mann-Whitney U test: ns, non-significant; *, $P < 0.05$; **, $P < 0.01$; ***, $P < 0.001$.

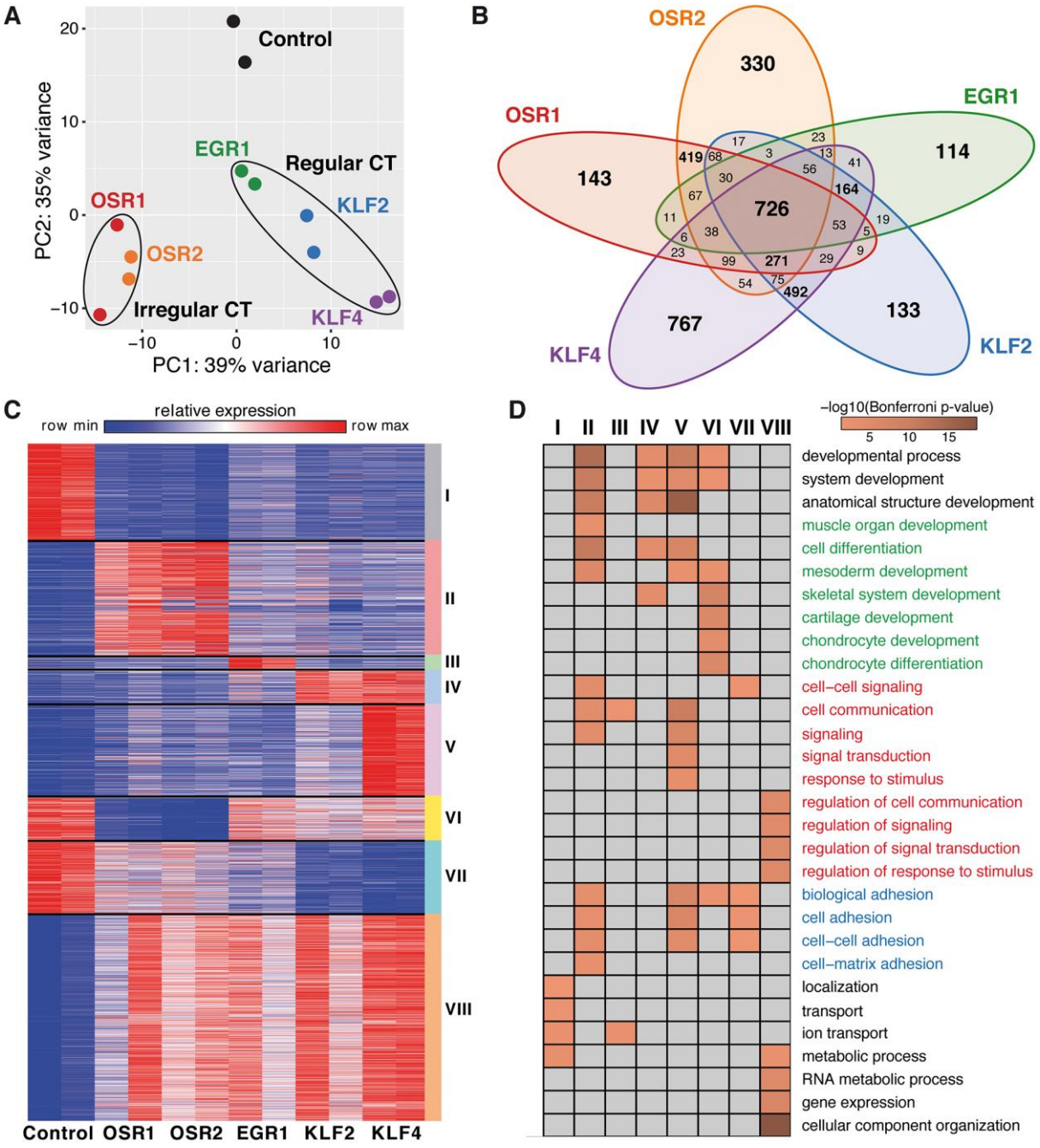

Fig. 3. Gene expression profiles in chMM cultures upon overexpression of CT-associated TFs. (A) PCA analysis on global gene expression profiles of TF-overexpressing chMM cultures. (B) Venn diagram of the 4,298 non-redundant DE genes detected across all TF-overexpressing chMM cultures. (C) Gene clusters identified by *K*-means partitioning on the 4,298 non-redundant DE genes. (D) GO analysis for biological processes of the DE genes belonging to each *K*-means cluster. GO terms related to cell differentiation and development

are depicted in green, cell signalling and communication in red, biological and cell adhesion in blue. Clusters having no significant enrichment for the specified GO terms are depicted in grey.

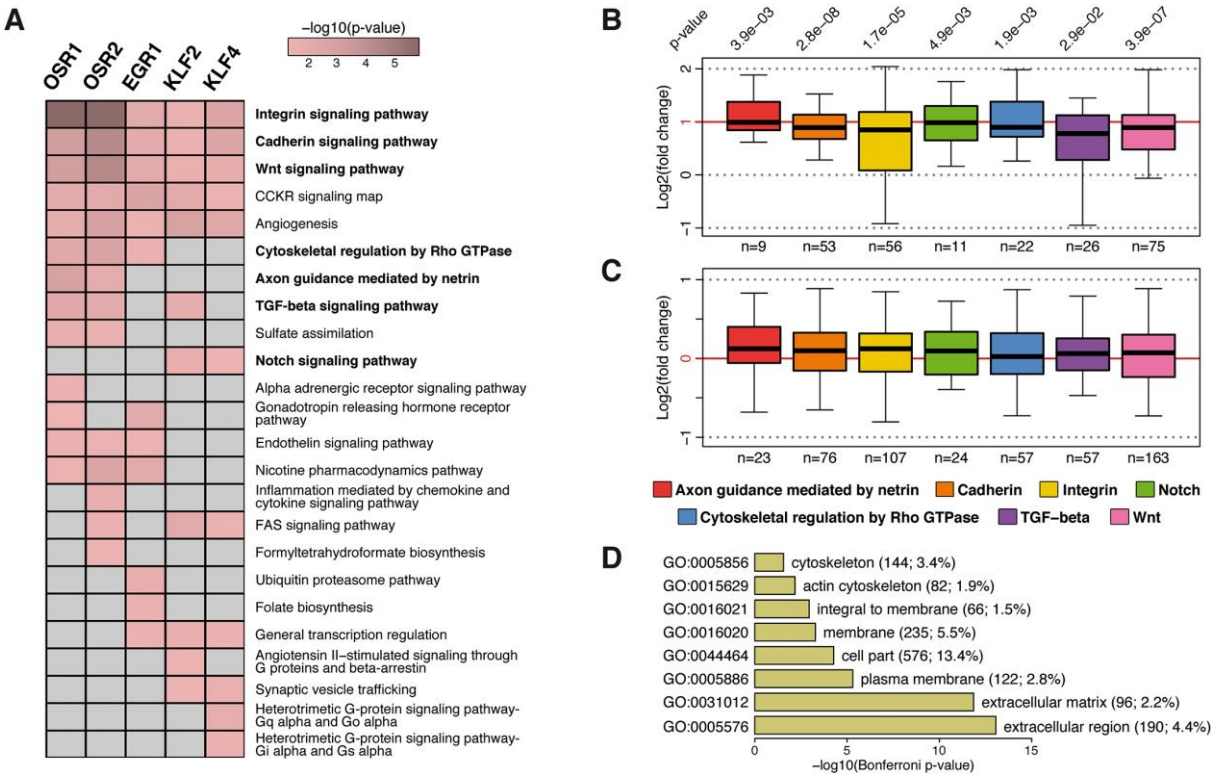

Fig. 4. Signalling signature enrichment analysis of DE genes. (A) Panther pathways overrepresented within the DE genes detected upon overexpression of each TF in chMM cultures. DE genes having no enrichment for the specified Panther pathway are depicted in grey. (B,C) Global expression levels of DE genes (B) and non-DE genes (C) belonging to the selected Panther pathways. Log2 fold changes of each gene were averaged across all chMM culture conditions and replicates. Number of genes (n) in each Panther pathway is indicated at the bottom of each box. Paired Wilcoxon rank-sum test: p-values are indicated at the top of each box. (D) Cellular component GO analysis of the 4,298 non-redundant DE genes.

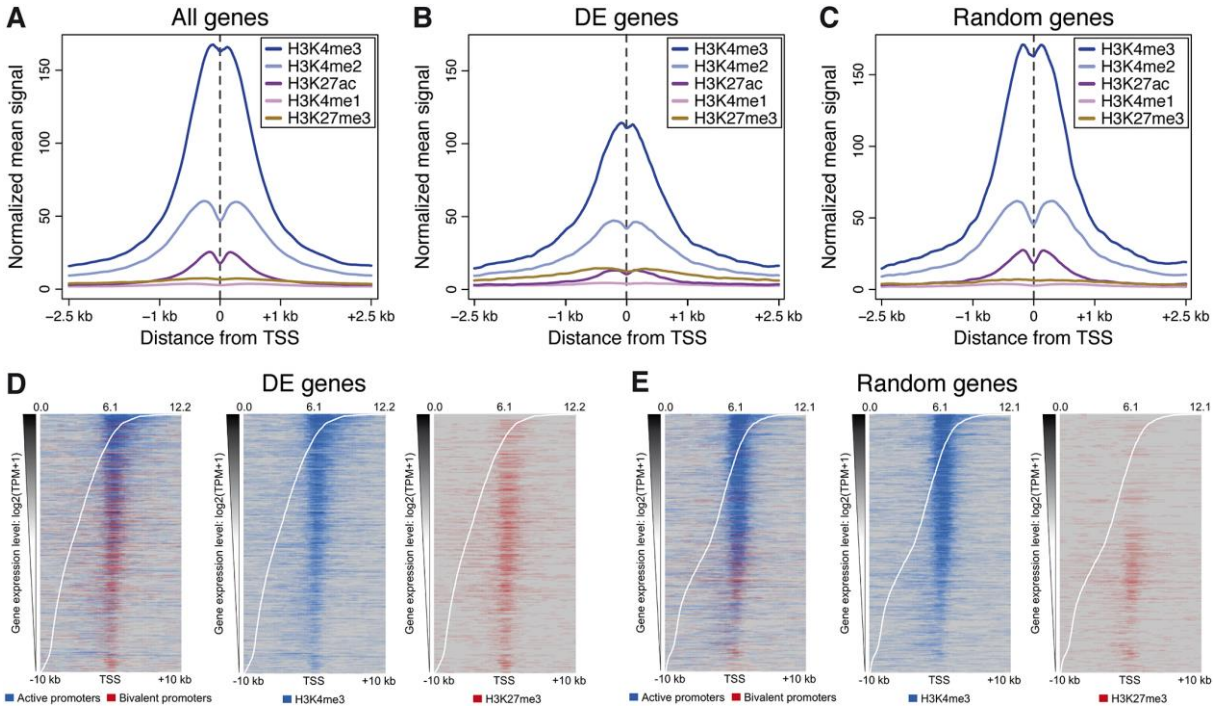

Fig. 5. Chromatin landscape in chMM cultures. (A-C) Normalized mean histone ChIP-seq signal surrounding the TSS of all genes (A), DE genes (B) and randomly selected genes (C). (D,E) Distribution of active (blue) and bivalent (red) promoter domains at the TSS of DE genes (D) and randomly selected genes (E). H3K4me3 (blue) signal is present in active and bivalent promoter domains, whereas H3K4me3 (red) signal is only detected in bivalent promoter domains. Intervals with a main regulatory domain being different from active and bivalent promoter are depicted in grey. Genes were ordered according to their expression levels (white curve).

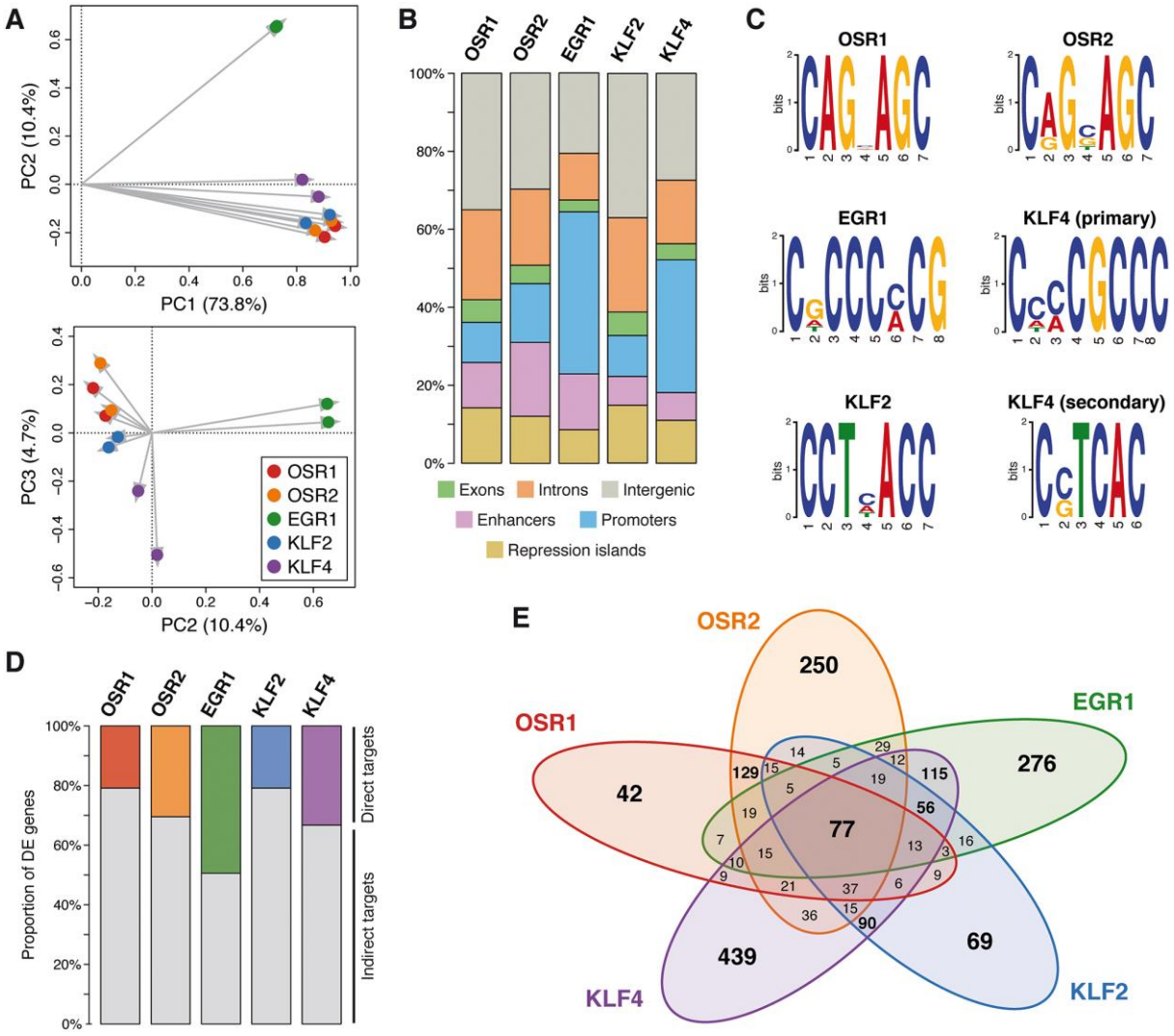

Fig. 6. Regulatory patterns of CT-associated TFs. (A) PCA analysis on the normalized ChIP-seq signal profiles of all TFs and biological replicates. (B) Proportion of TFBS in chromatin domains and gene features. (C) TF recognition motifs. (D) Proportion of direct and indirect target genes of each TF in chMM cultures. (E) Venn diagram of the 1,858 non-redundant direct target genes detected across all TF-overexpressing chMM cultures.

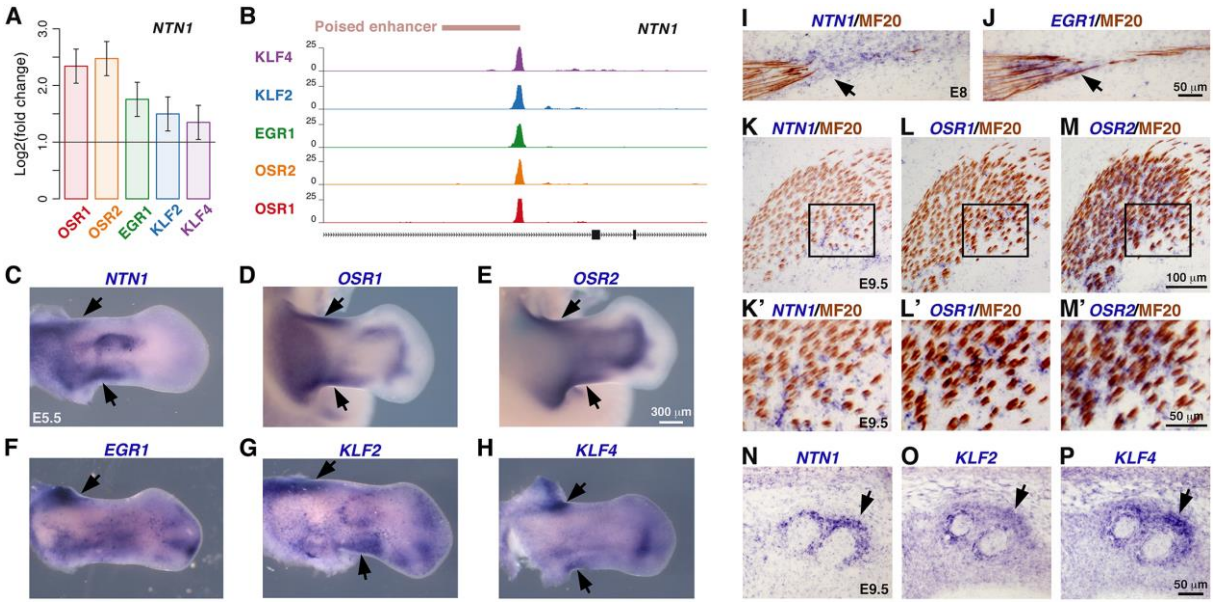

Fig. 7. *NTN1* is a common target gene to the five CT-associated TFs. (A) *NTN1* expression levels in TF-overexpressing chMM cultures determined by RNA-seq. (B) Binding site for the five TFs identified by ChIP-seq within an intronic enhancer of *NTN1* gene. (C-H) Whole-mount in situ hybridization to hindlimbs of E5.5 chick embryos with *NTN1* (C), *OSR1* (D), *OSR2* (E), *EGR1* (F), *KLF2* (G) and *KLF4* (H) probes (blue). (I-P) In situ hybridization to forelimbs of E8 (I,J) and E9.5 (K-P) chick embryos followed by immunohistochemistry with the MF20 antibody (brown). (I,J) Adjacent and longitudinal limb sections were hybridized with *NTN1* (I) and *EGR1* (J) probes (blue). (K-P) Adjacent and transverse limb sections were hybridized with *NTN1* (K,K',N), *OSR1* (L,L'), *OSR2* (M,M'), *KLF2* (O) and *KLF4* (P) probes (blue). (K',L',M') are higher magnifications of the boxed areas in (K,L,M), respectively. Areas of overlapping expression are indicated by arrows.

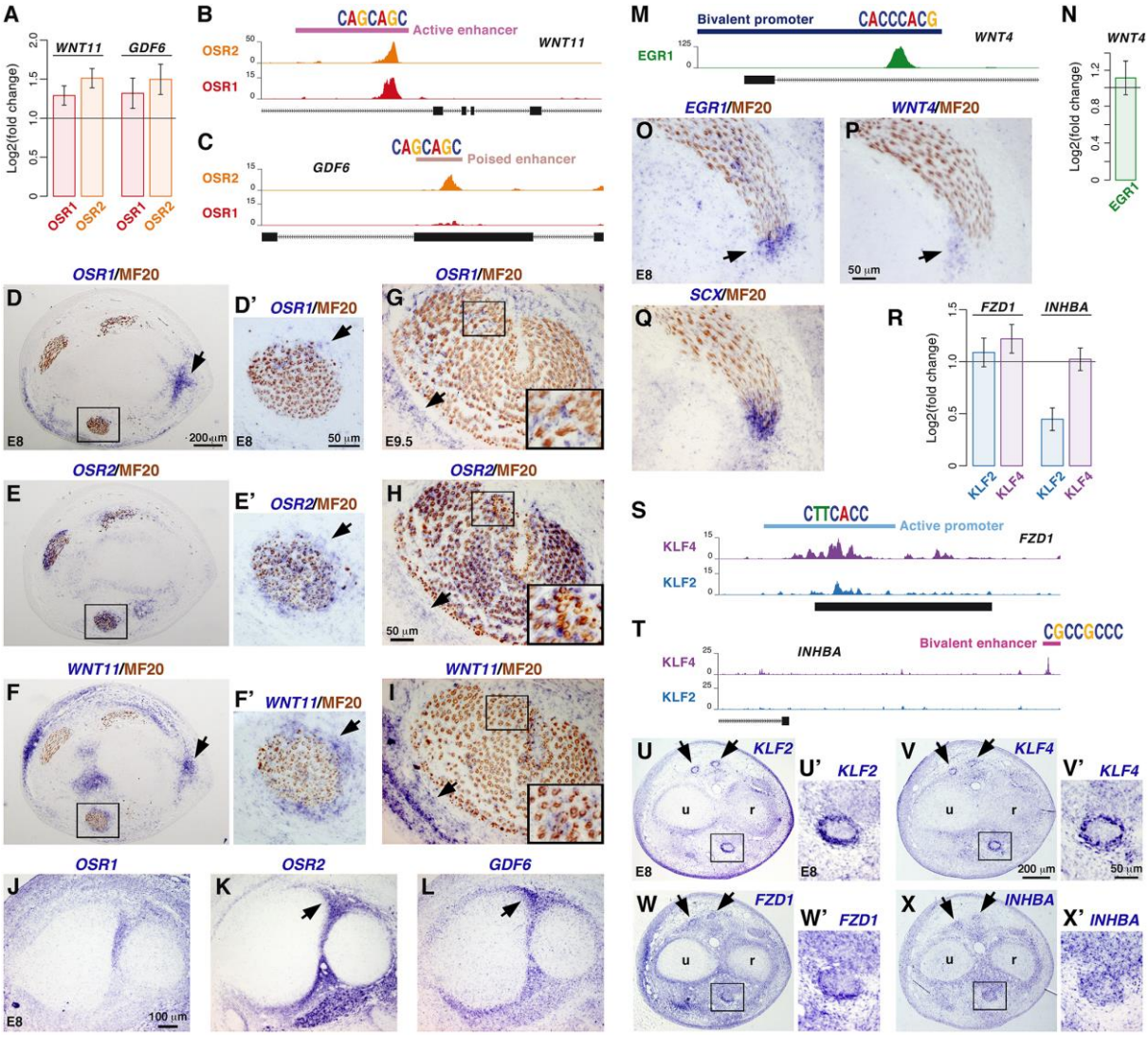

Fig. 8. Selection of target genes encoding signalling molecules downstream of the five CT-associated TFs. (A) *WNT11* and *GDF6* expression levels in OSR1- and OSR2-overexpressing chMM cultures determined by RNA-seq. (B) Binding site and motif for OSR1 and OSR2 identified by ChIP-seq within an intronic enhancer of *WNT11* gene. (C) Binding site and motif for OSR2 identified by ChIP-seq within an exonic enhancer of *GDF6* gene. (D-I) In situ hybridization to forelimbs of E8 (D-F') and E9.5 (G-I) chick embryos followed by immunohistochemistry with the MF20 antibody (brown). Adjacent and transverse limb sections were hybridized with *OSR1* (D,D',G), *OSR2* (E,E',H) and *WNT11* (F,F',I) probes (blue). (D',E',F') are higher magnifications of the boxed areas in (D,E,F), respectively. (J-L) In situ

hybridization to adjacent and transverse forelimb sections of E8 chick embryos with *OSR1* (J), *OSR2* (K) and *GDF6* (L) probes (blue). (M) Binding site and motif for EGR1 identified by ChIP-seq within the promoter of *WNT4* gene. (N) *WNT4* expression levels in EGR1-overexpressing chMM cultures determined by RNA-seq. (O-Q) In situ hybridization to adjacent and transverse forelimb sections of E8 chick embryos with *EGR1* (O), *WNT4* (P) and *SCX* (Q) probes (blue) followed by immunohistochemistry with the MF20 antibody (brown). (R) *FZD1* and *INHBA* expression levels in KLF2- and KLF4-overexpressing chMM cultures determined by RNA-seq. (S) Binding site and motif for KLF2 and KLF4 identified by ChIP-seq within the promoter of *FZD1* gene. (T) Binding site and motif for KLF4 identified by ChIP-seq within an enhancer located upstream of *INHBA* gene. (U-X') In situ hybridization to adjacent and transverse forelimb sections of E8 chick embryos with *KLF2* (U,U'), *KLF4* (V,V'), *FZD1* (W,W') and *INHBA* (X,X') probes (blue). (U',V',W',X') are higher magnifications of the boxed areas in (U,V,W,X), respectively. Areas of overlapping expression are indicated by arrows. u, ulna; r, radius.

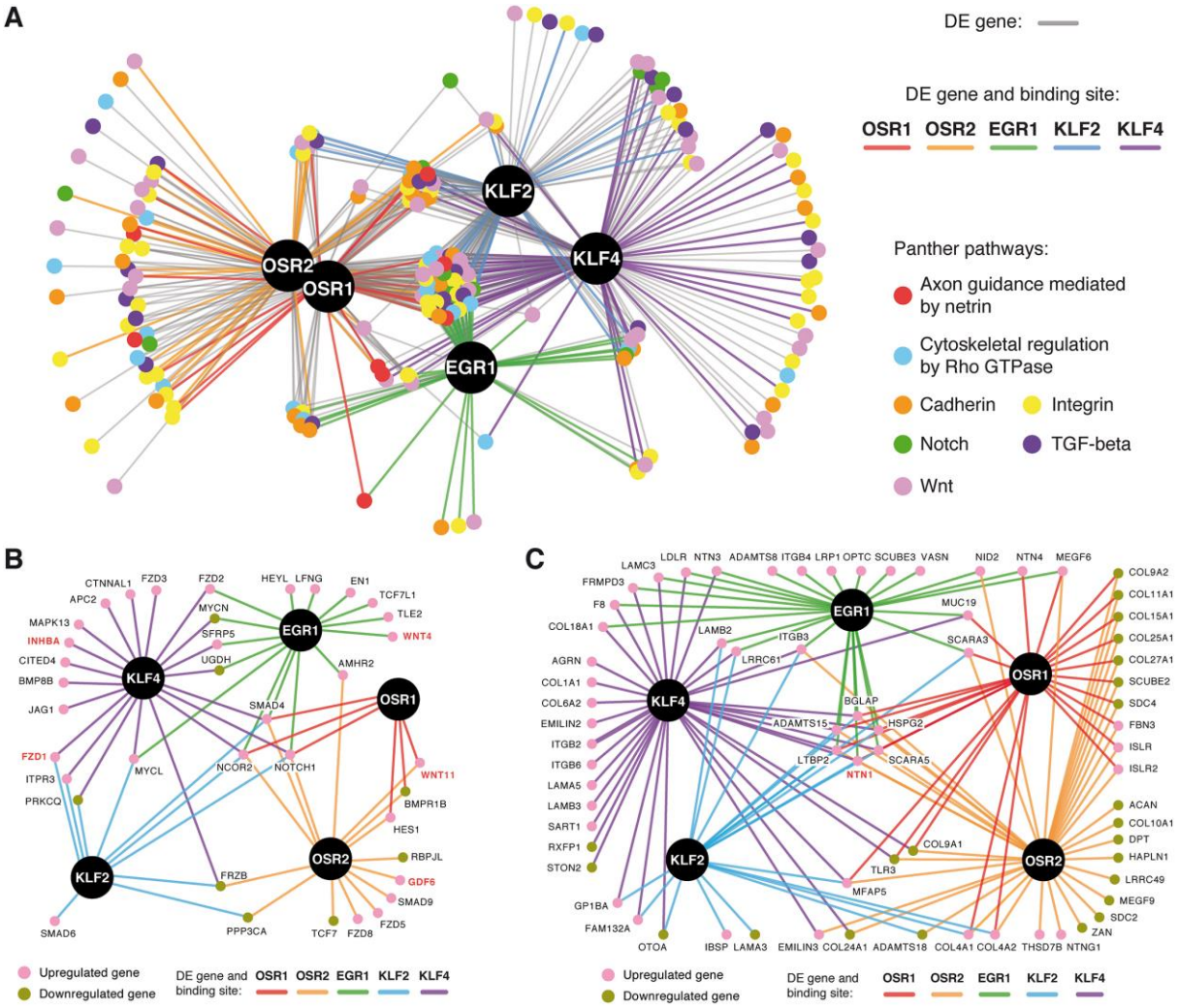

Fig. 9. Regulatory networks of CT-associated TFs. (**A**) Transcriptional regulatory network of the CT-associated TFs and their target genes related to the indicated signalling pathways. Coloured connections correspond to direct interactions between the TFs and their target genes (DE gene and TFBS), while indirect interactions are depicted in grey (DE gene only). (**B**) Network representation of the 38 target genes associated with the Notch, TGF-β and Wnt signalling pathways that are directly regulated by the TFs. (**C**) Network representation of the 70 target genes associated with the ECM that are directly regulated by the TFs. Genes depicted in red correspond to the selected target genes investigated by in situ hybridization.

Supplementary Figures

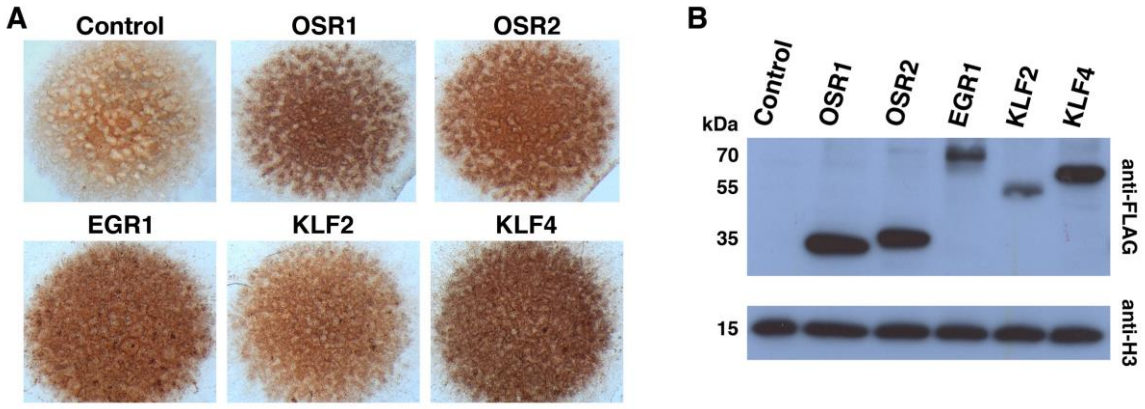

Fig. S1. Detection of the 3F-tagged TFs within the chMM cultures. (A) Immunohistochemistry with an anti-FLAG antibody to detect the infection level of retroviral RCAS-BP(A) particles carrying each of the TF CDS fused at their 3'-end with the 3F tag. (B) Western blot analysis of the 3F-tagged recombinant TFs overexpressed in chMM cultures. TFs were detected by using an anti-FLAG antibody. Protein amount in each loaded sample was controlled by using an anti-H3 antibody recognizing histone proteins H3.

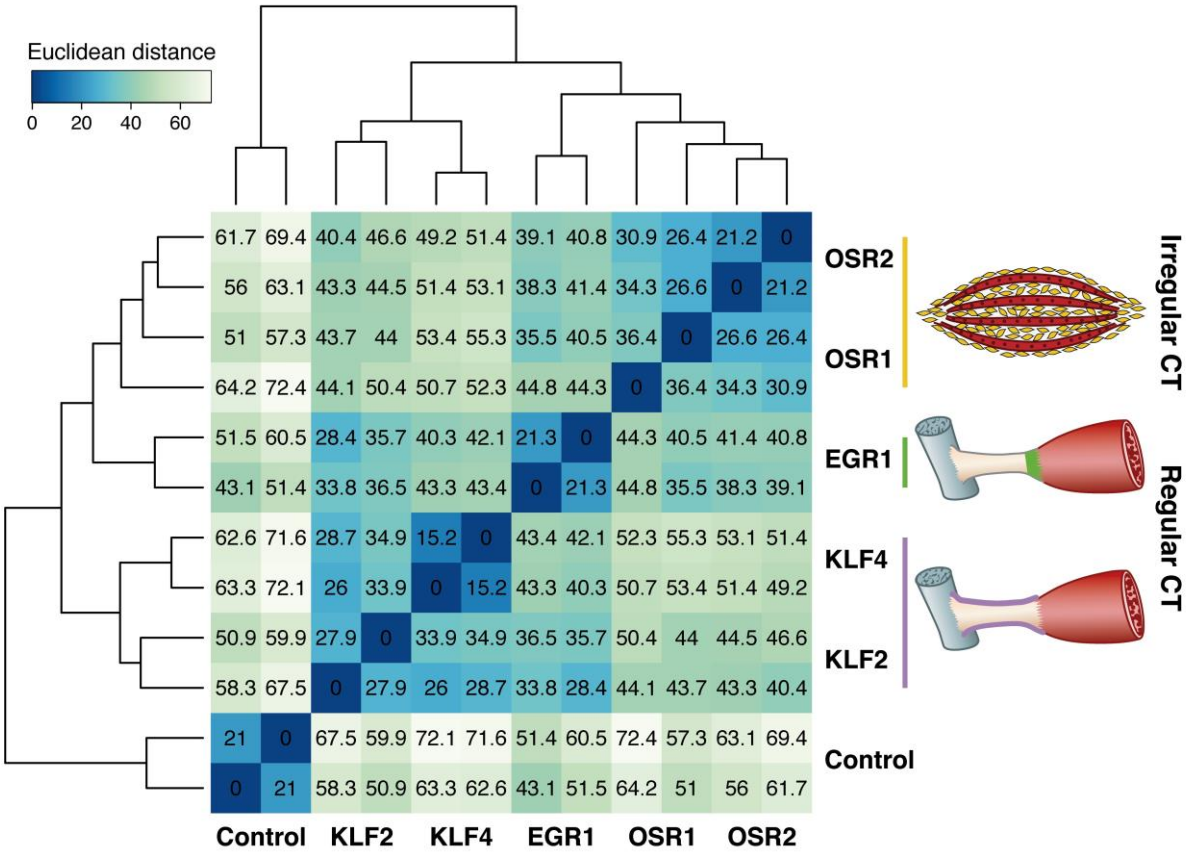

Fig. S2. Sample-to-sample distance across TF-overexpressing chMM cultures. Euclidean distances were calculated across all biological replicates and conditions.

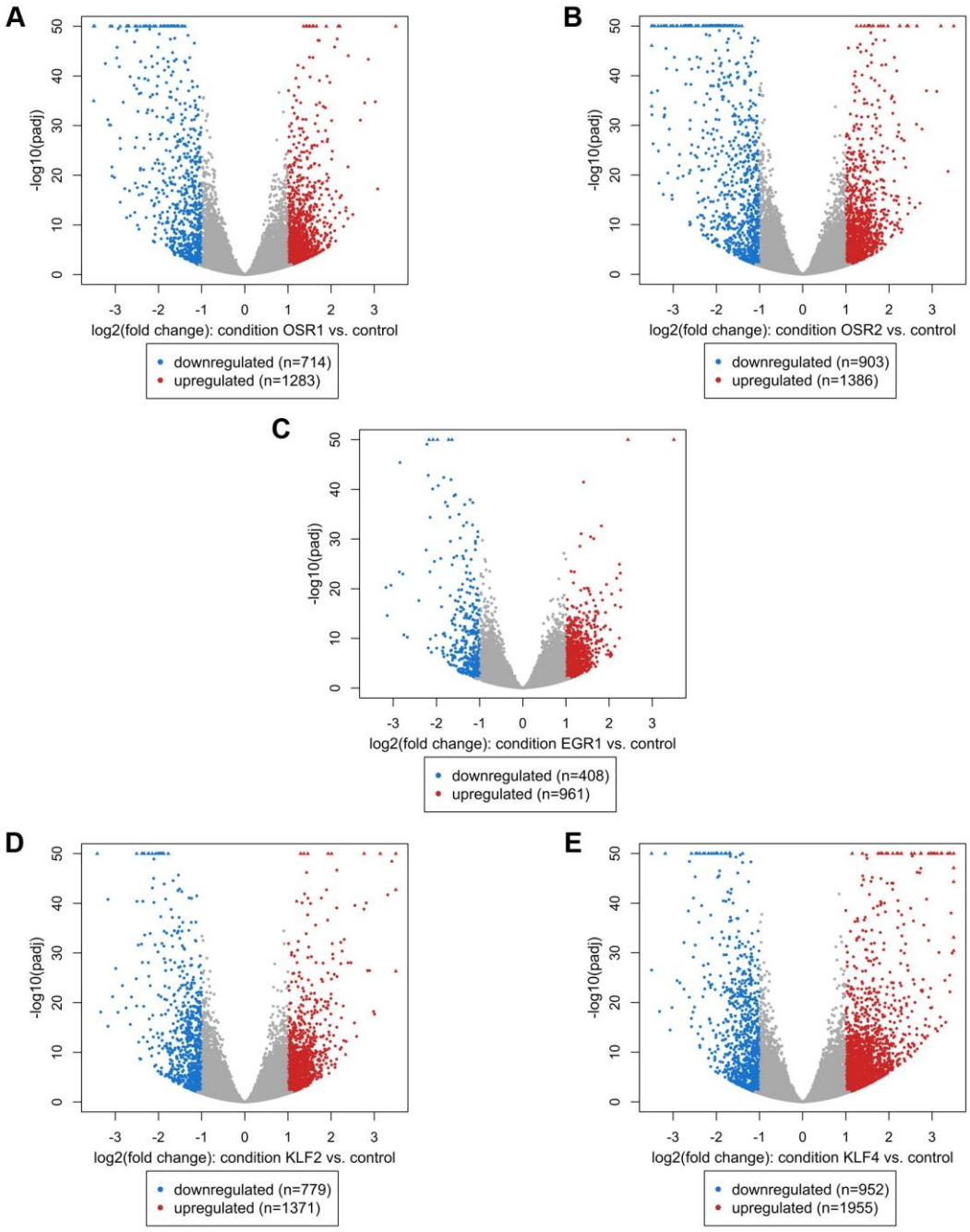

Fig. S3. DE genes detected in TF-overexpressing chMM cultures. Volcano plots of the 10,712 DE genes detected in the chMM cultures overexpressing OSR1 (A), OSR2 (B), EGR1 (C), KLF2 (D) and KLF4 (E). (A) 1,997 DE genes detected upon OSR1 overexpression. (B) 2,289 DE genes detected upon OSR2 overexpression. (C) 1,369 DE genes detected upon EGR1 overexpression. (D) 2,150 DE genes detected upon KLF2 overexpression. (E) 2,907 DE genes detected upon KLF4 overexpression.

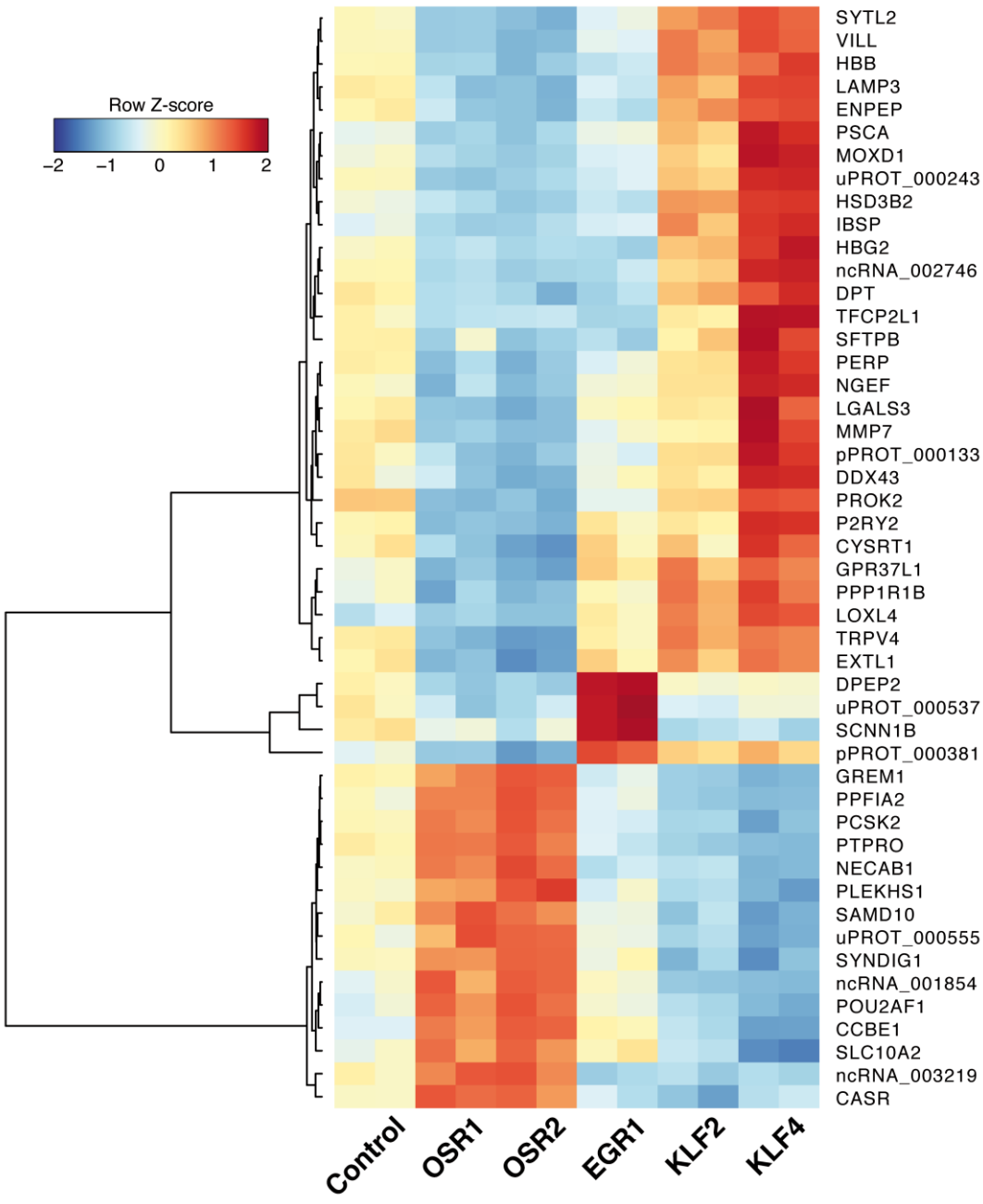

Fig. S4. Consistency among the TF regulatory patterns. Heatmap of the 48 shared DE genes regulated in opposite directions across all chMM cultures.

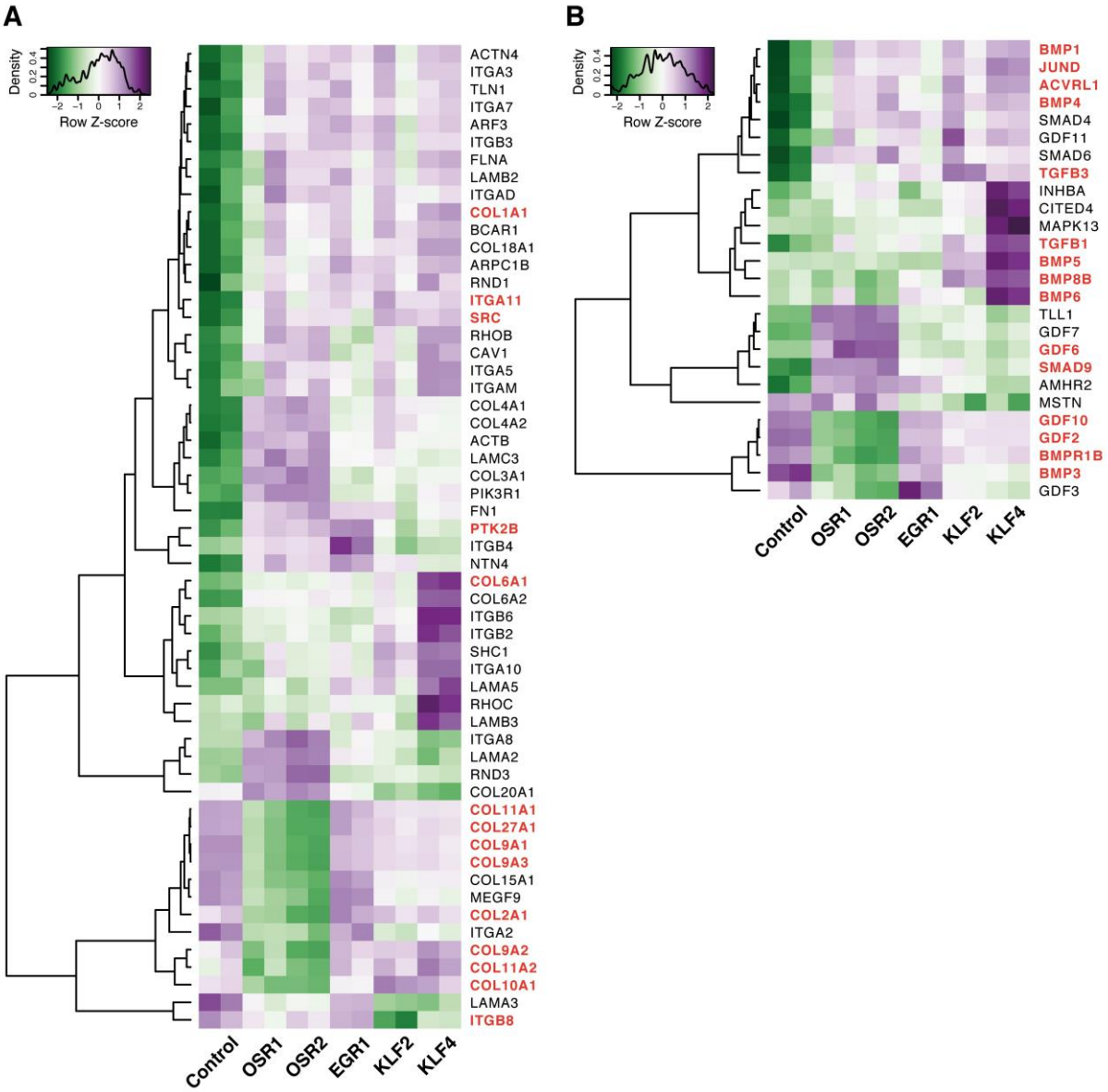

Fig. S5. DE genes associated with the Integrin and TGF-β signalling pathways. (A) Heatmap of the 56 DE genes associated with the Panther Integrin signalling pathway. (B) Heatmap of the 26 DE genes associated with the Panther TGF-β signalling pathway. Genes depicted in red are associated with GO terms related to cartilage and bone development.

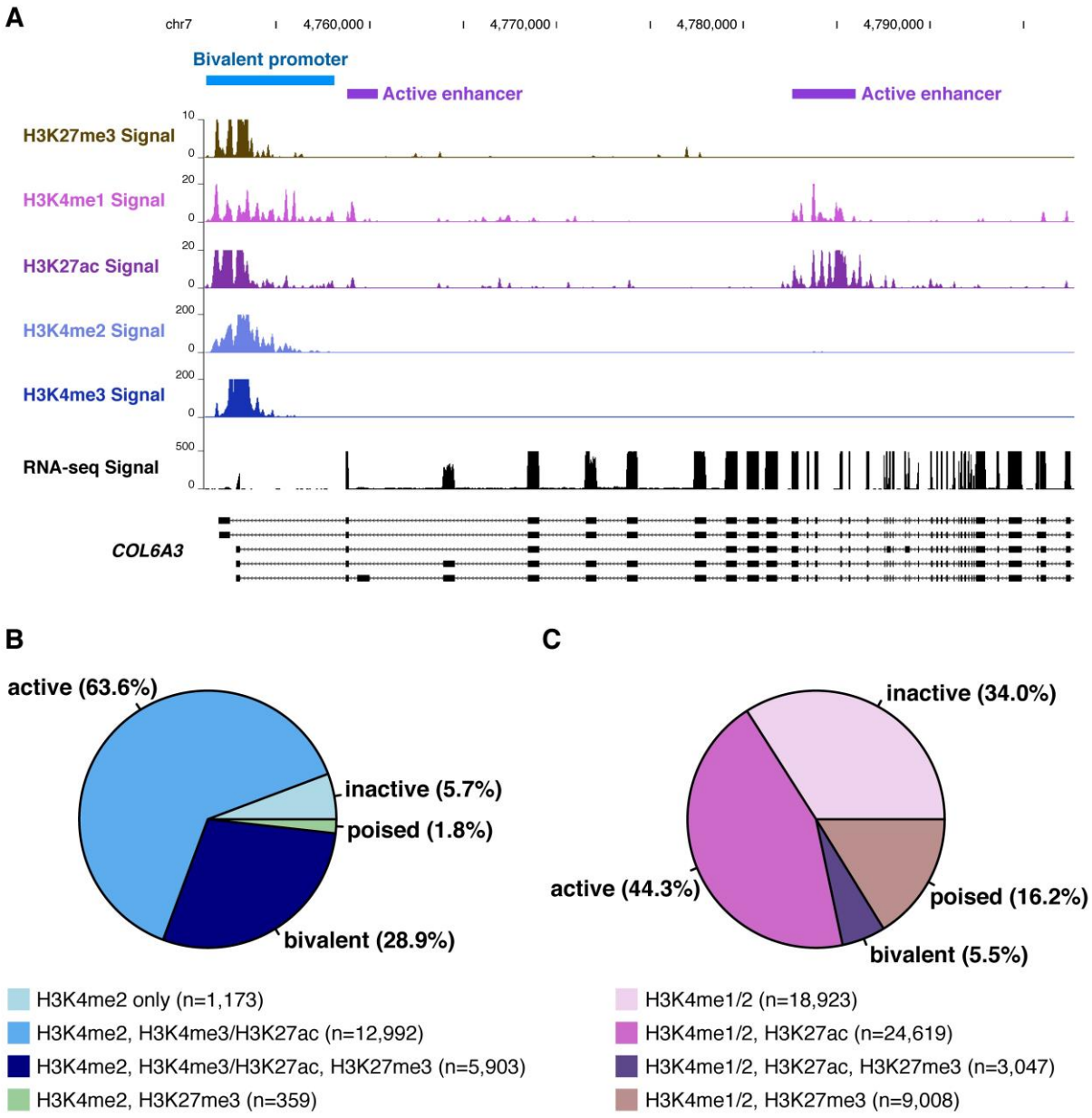

Fig. S6. Chromatin regulatory landscape in chMM cultures. (A) Chromatin landscape in the vicinity of *COL6A3* gene in chMM cultures. Five covalent histone tail modifications were investigated genome-widely in chMM cultures infected with retroviruses carrying no recombinant protein: H3K4me2 (blue), H3K4me3 (dark blue), H3K4me1 (pink), H3K27ac (dark purple) and H3K27me3 (brown). (B) Promoter regulatory domains. 20,427 promoters were identified and divided into four chromatin states: inactive (light blue), poised (green), active (blue) and bivalent (dark blue). (C) Enhancer regulatory domains. 55,597 enhancers were identified and divided into four chromatin states: inactive (light pink), poised (brown), active (purple) and bivalent (dark purple).

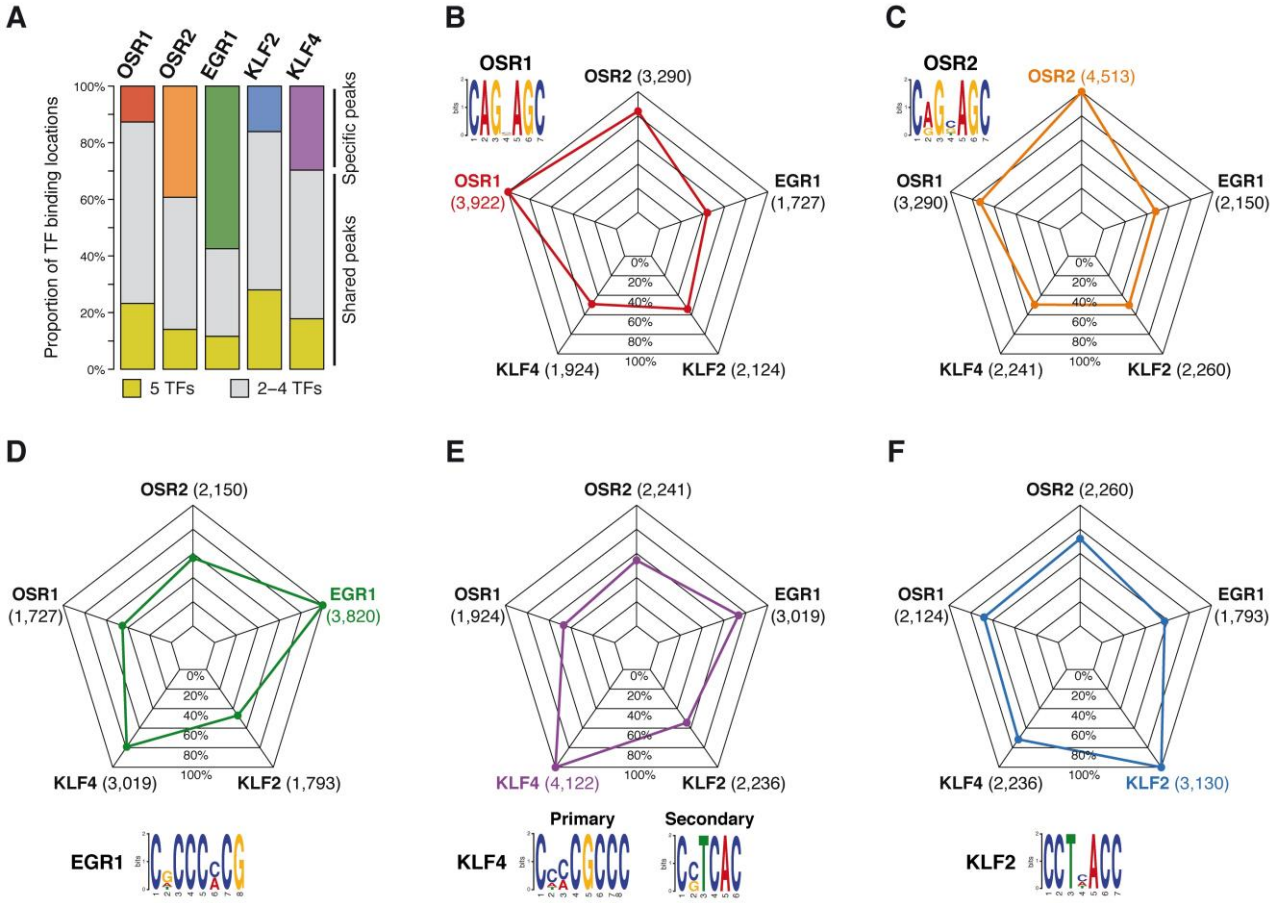

Fig. S7. Genome-wide TF binding patterns. (A) Proportion of TF binding regions specific to a single TF and shared by multiple TFs. (B-F) Pairwise comparisons of shared occupancy among the five TFs for OSR1 (B), OSR2 (C), EGR1 (D), KLF4 (E) and KLF2 (F).

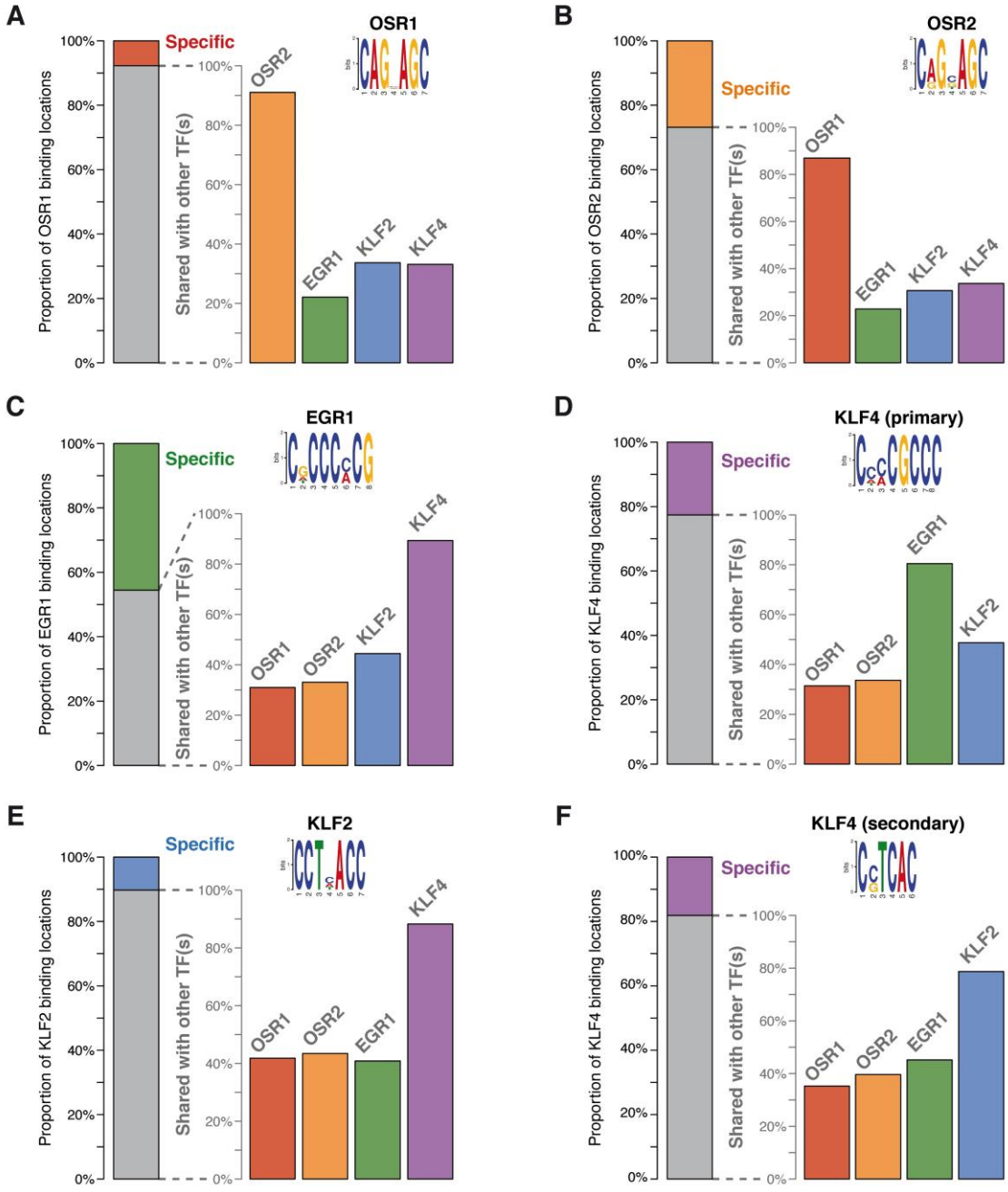

Fig. S8. TF occupancy among shared target genes. (A,B) Pairwise comparisons of TF occupancy among the 318 direct target genes shared by OSR1 and OSR2 for OSR1 (A) and OSR2 (B) binding locations. (C,D) Pairwise comparisons of TF occupancy among the 317 direct target genes shared by EGR1 and KLF4 for EGR1 (C) and KLF4 (D) binding locations. (E,F) Pairwise comparisons of TF occupancy among the 313 direct target genes shared by KLF2 and KLF4 for KLF2 (E) and KLF4 (F) binding locations.

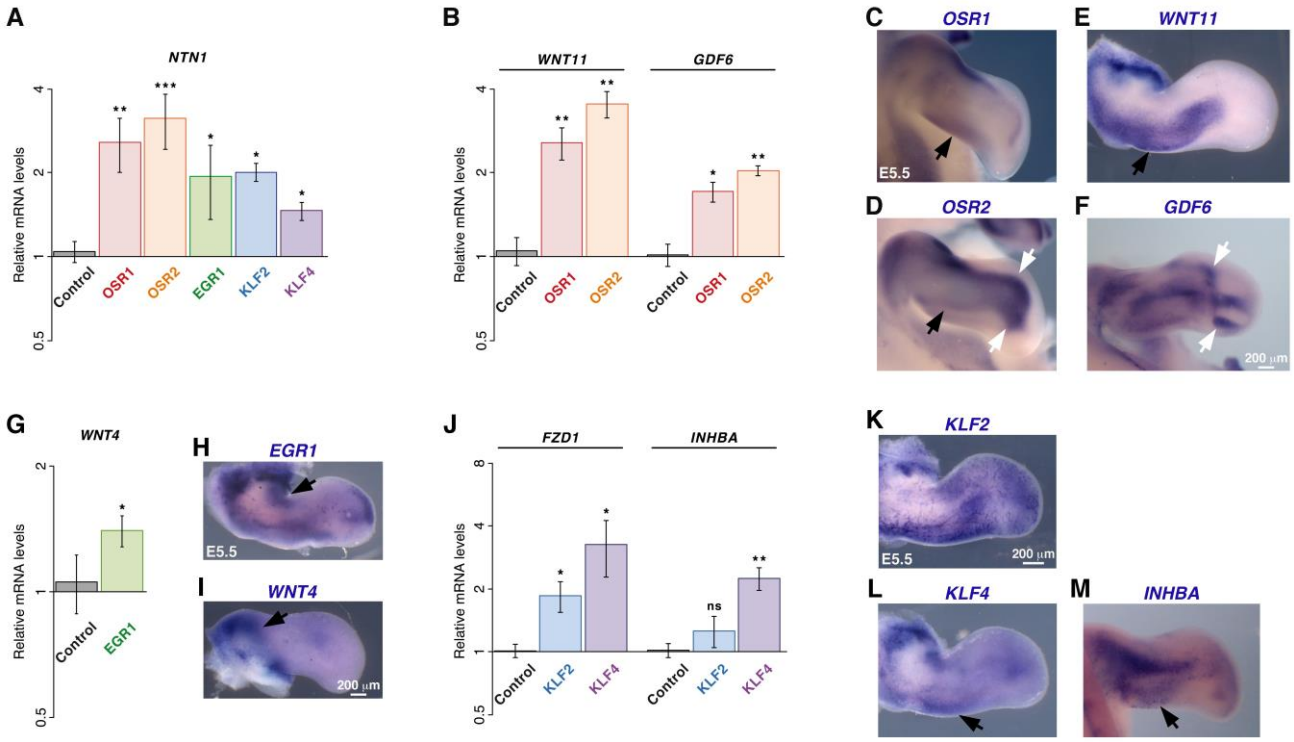

Fig. S9. Validation of selected candidate target genes. (A) Quantitative RT-PCR analysis of *NTN1* expression in TF-overexpressing chMM cultures. (B) Quantitative RT-PCR analysis of *WNT11* and *GDF6* expression in OSR1- and OSR2-overexpressing chMM cultures. (C-F) Whole-mount in situ hybridization to forelimbs of E5.5 chick embryos with *OSR1* (C), *OSR2* (D), *WNT11* (E) and *GDF6* (F) probes (blue). Black arrows indicate *OSR1*, *OSR2* and *WNT11* overlapping expression domains, while white arrows indicate *OSR2* and *GDF6* overlapping expression domains. (G) Quantitative RT-PCR analysis of *WNT4* expression in EGR1-overexpressing chMM cultures. (H,I) Whole-mount in situ hybridization to forelimbs of E5.5 chick embryos with *EGR1* (H) and *WNT4* (I) probes (blue). Areas of overlapping expression are indicated by arrows. (J) Quantitative RT-PCR analysis of *FZD1* and *INHBA* expression in KLF2- and KLF4-overexpressing chMM cultures. (K-M) Whole-mount in situ hybridization to forelimbs of E5.5 chick embryos with *KLF2* (K), *KLF4* (L) and *INHBA* (M) probes (blue). Areas of overlapping expression are indicated by arrows. (A,B,G,J) Quantitative RT-PCR graphs depict relative mRNA levels: mean ± SEM; two-tailed Mann-Whitney U test: ns, non-significant; *, $P < 0.05$; **, $P < 0.01$; ***, $P < 0.001$.

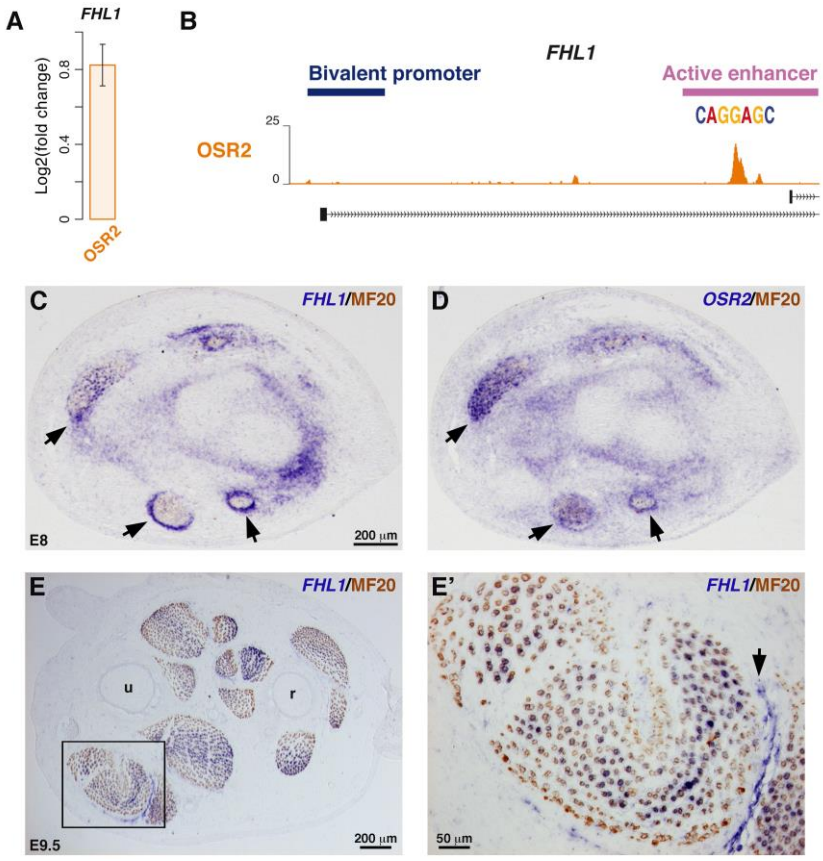

Fig. S10. *FHL1* as direct target of OSR2. (A) *FHL1* expression levels in OSR2-overexpressing chMM cultures determined by RNA-seq. (B) Binding site and motif for OSR2 identified by ChIP-seq within an intronic enhancer of *FHL1* gene. (C-E') In situ hybridization to forelimbs of E8 (C,D) and E9.5 (E,E') chick embryos followed by immunohistochemistry with the MF20 antibody (brown). (C,D) Adjacent and transverse limb sections were hybridized with *FHL1* (C) and *OSR2* (D) probes (blue). Areas of overlapping expression are indicated by arrows. (E,E') Transverse limb sections were hybridized with *FHL1* probes (blue). *FHL1* is expressed in $MF20^{+}$ myotubes, but also in CT (arrow). (E') is a higher magnification of the boxed area in (E). u, ulna; r, radius.

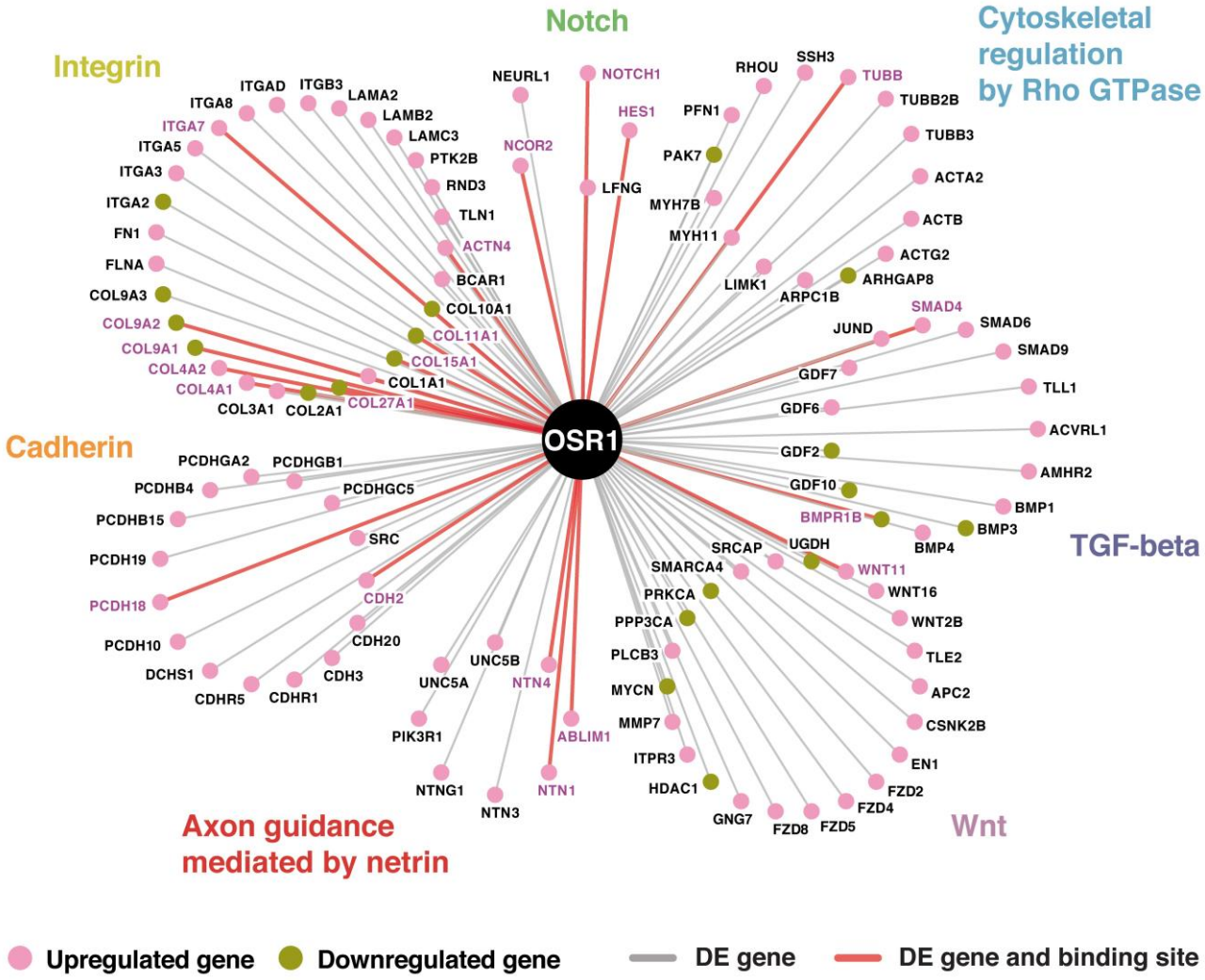

Fig. S11. Molecular signatures regulated by OSR1. Circular representation of DE genes identified in chMM cultures upon OSR1 overexpression that are associated with the selected Panther signalling pathways. Downregulated genes are depicted as brown nodes and upregulated genes as pink nodes. Connections in red correspond to direct interactions between OSR1 and its target genes, while indirect interactions are depicted in grey.

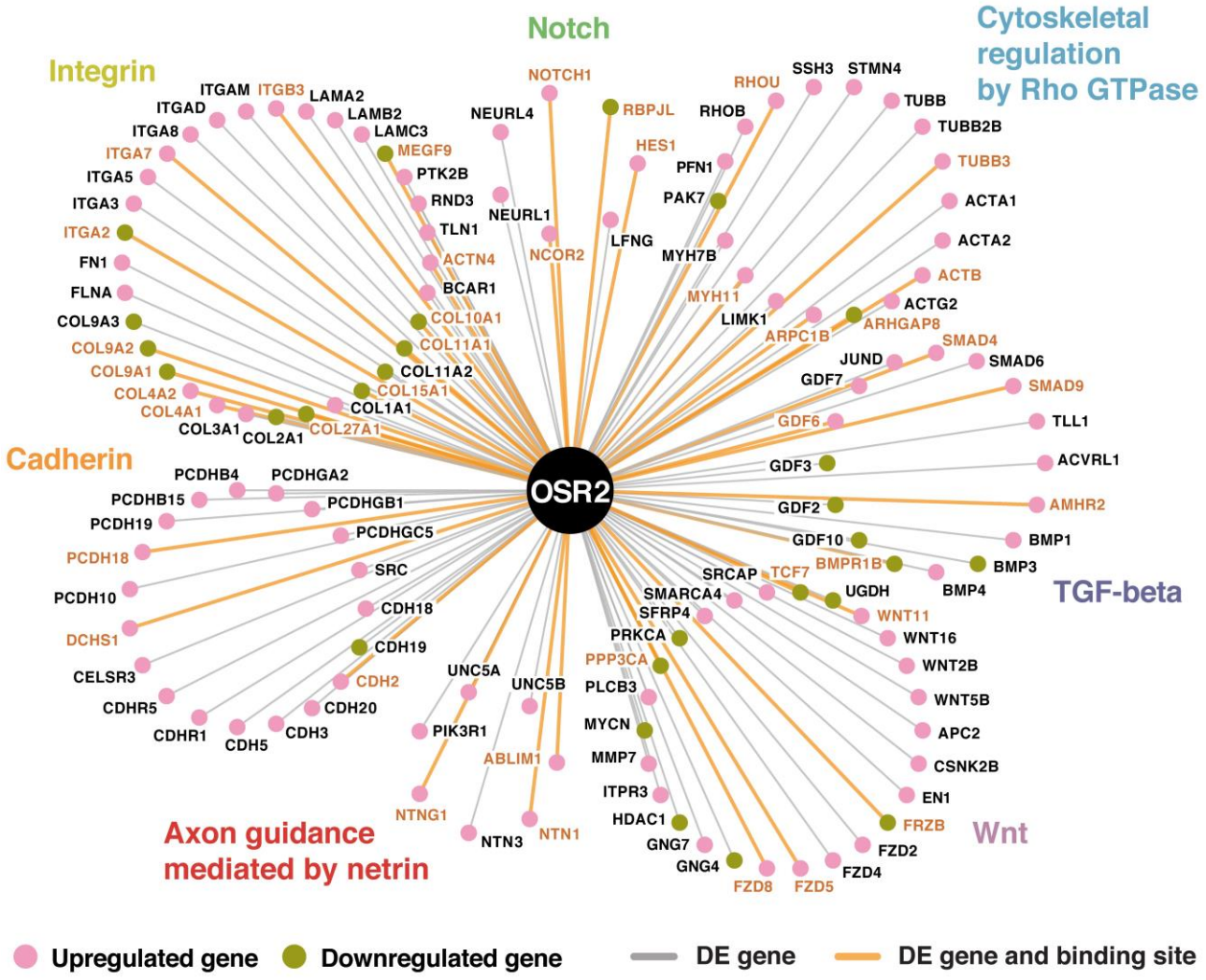

Upregulated gene Downregulated gene DE gene DE gene and binding site

Fig. S12. Molecular signatures regulated by OSR2. Circular representation of DE genes identified in chMM cultures upon OSR2 overexpression that are associated with the selected Panther signalling pathways. Downregulated genes are depicted as brown nodes and upregulated genes as pink nodes. Connections in orange correspond to direct interactions between OSR2 and its target genes, while indirect interactions are depicted in grey.

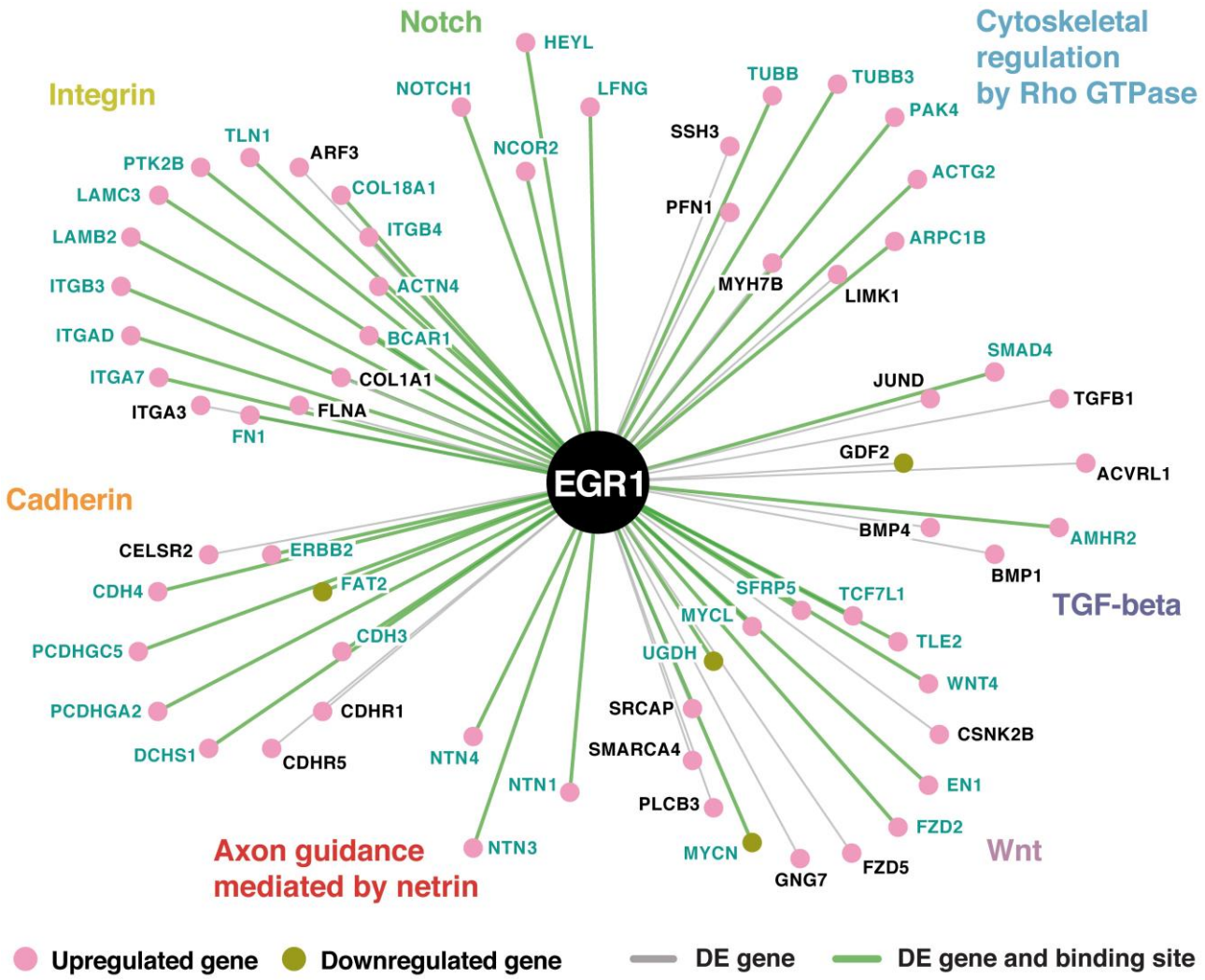

Fig. S13. Molecular signatures regulated by EGR1. Circular representation of DE genes identified in chMM cultures upon EGR1 overexpression that are associated with the selected Panther signalling pathways. Downregulated genes are depicted as brown nodes and upregulated genes as pink nodes. Connections in green correspond to direct interactions between EGR1 and its target genes, while indirect interactions are depicted in grey.

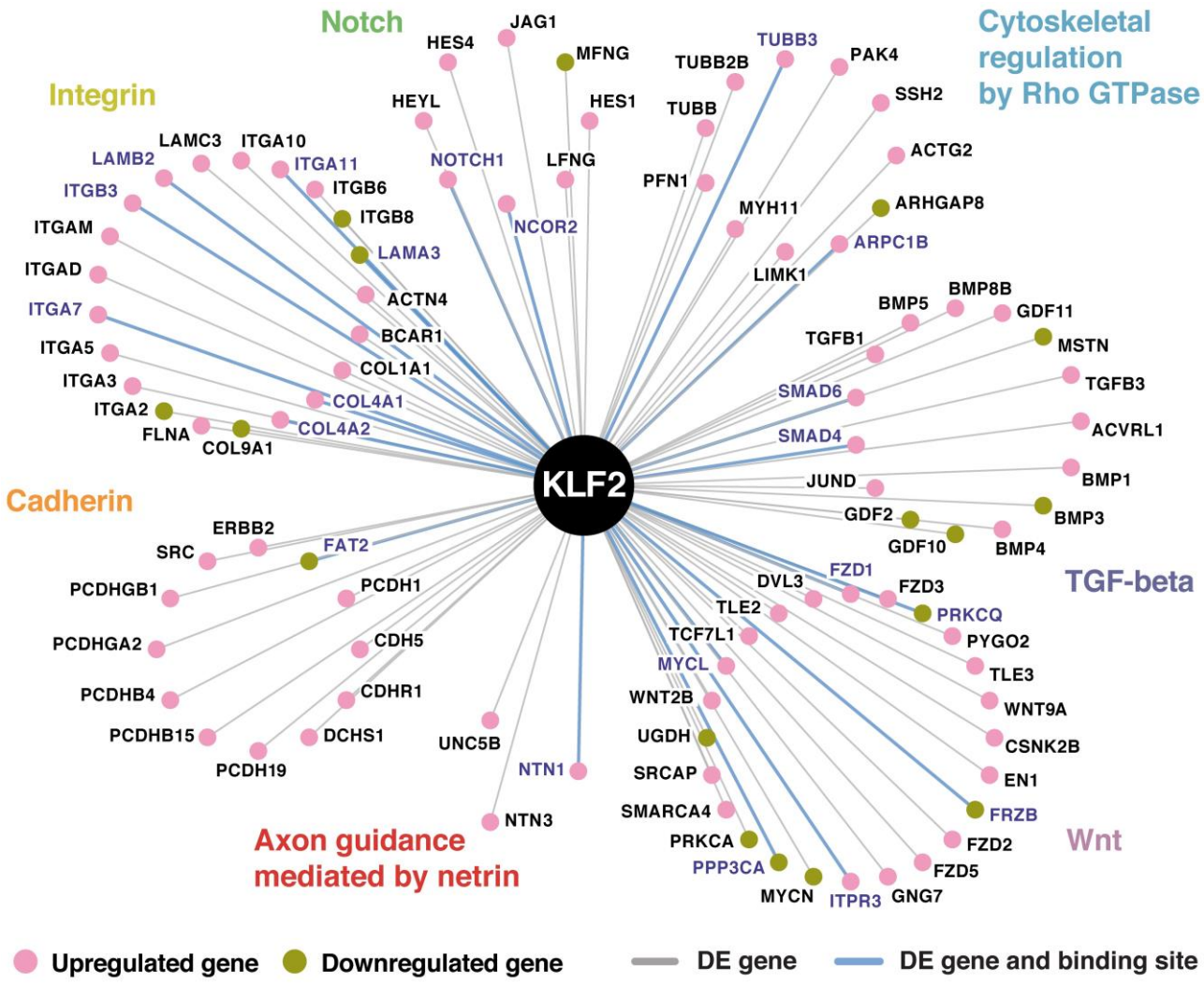

Fig. S14. Molecular signatures regulated by KLF2. Circular representation of DE genes identified in chMM cultures upon KLF2 overexpression that are associated with the selected Panther signalling pathways. Downregulated genes are depicted as brown nodes and upregulated genes as pink nodes. Connections in blue correspond to direct interactions between KLF2 and its target genes, while indirect interactions are depicted in grey.

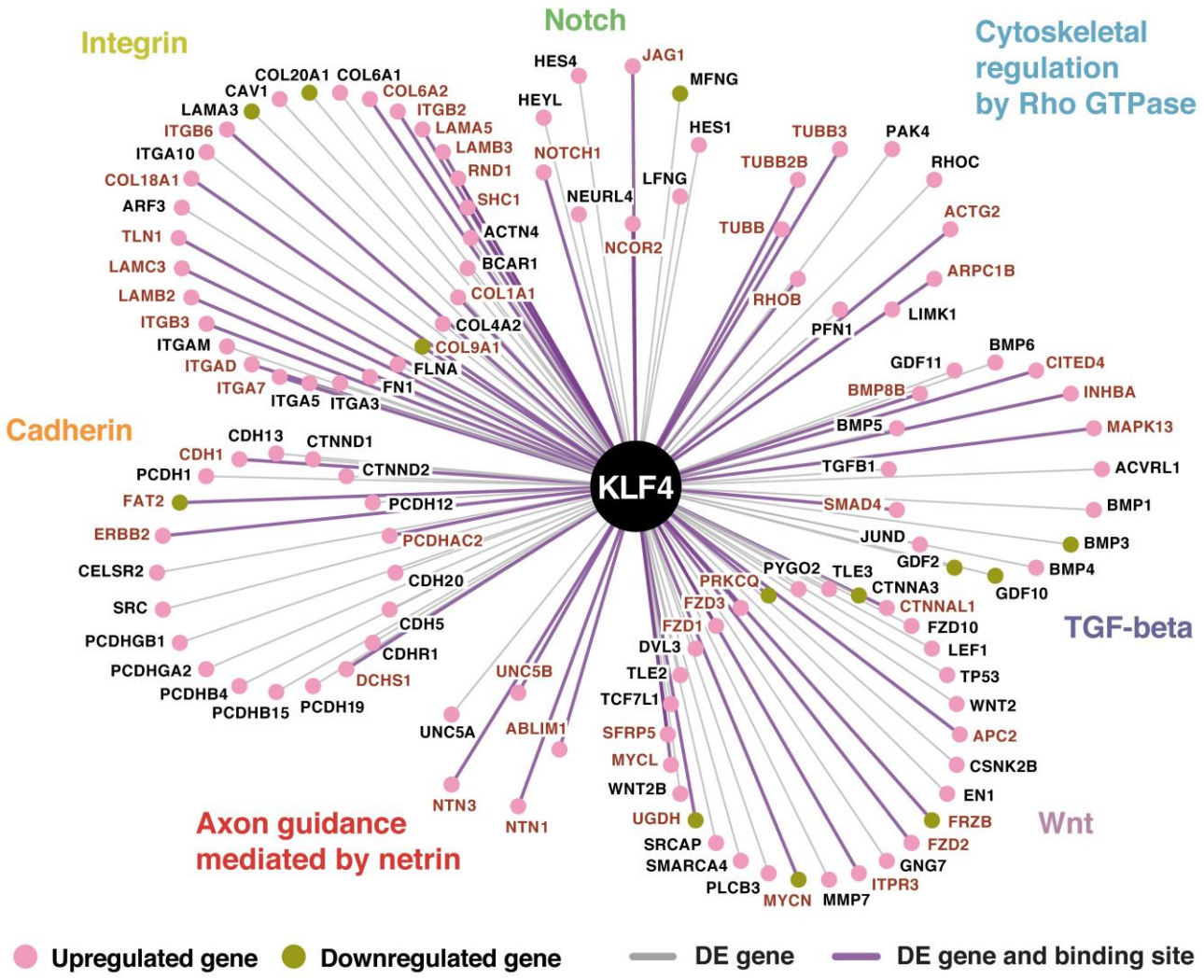

Fig. S15. Molecular signatures regulated by KLF4. Circular representation of DE genes identified in chMM cultures upon KLF4 overexpression that are associated with the selected Panther signalling pathways. Downregulated genes are depicted as brown nodes and upregulated genes as pink nodes. Connections in purple correspond to direct interactions between KLF4 and its target genes, while indirect interactions are depicted in grey.

Supplementary Tables

Table S1. Table combining RNA-seq and ChIP-seq data.

Click here to Download Table S1

Table S2. List of primers.

Click here to Download Table S2

Table S3. RNA-seq mapping and assignment metrics.

Click here to Download Table S3

Table S4. Histone modification ChIP-seq metrics.

Click here to Download Table S4

Table S5. Transcription Factor ChIP-seq metrics.

Click here to Download Table S5